On-line Tools for Assessing Petroleum Releases

by

James W. Weaver
Ecosystems Research Division
National Exposure Research Laboratory
Athens, Georgia 30605

Notice

Foreword

The National Exposure Research Laboratory's Ecosystems Research Division (ERD) in Athens, Georgia, conducts research on organic and inorganic chemicals, greenhouse gas biogeochemical cycles, and land use perturbations that create direct and indirect, chemical and non-chemical stresses, exposures, and potential risks to humans and ecosystems. ERD develops, tests, applies and provides technical support for exposure and ecosystem response models used for assessing and managing risks to humans and ecosystems, within a watershed / regional context.

The Regulatory Support Branch (RSB) conducts problem-driven and applied research, develops technology tools, and provides technical support to customer Program and Regional Offices, States, Municipalities, and Tribes. Models are distributed and supported via the EPA Center for Exposure Assessment Modeling (CEAM).

The Internet tools described in this report provide methods and models for evaluation of contaminated sites. Two problems are addressed by models. The first is the placement of wells for correct delineation of contaminant plumes. Because aquifer recharge can displace plumes downward, the vertical placement of well screens is critical to obtain proper characterization data. The second is the use of models where data are limited. In this case some form of uncertainty analysis is necessary to evaluate transport behavior. The remainder of the report describes a series of tools for estimating various model input parameters.

Rosemarie C. Russo, Ph.D.
Director
Ecosystems Research Division
Athens, Georgia

Table of Contents

List of Figures

List of Tables

1. Introduction

Sites that are contaminated with fuels and dissolved components of petroleum products are commonly assessed through a combination of field data collection and application of models. The field data typically consist of two types: first, field-measured aquifer parameters and second, contaminant and water level observations. The first type may consist of grain size distributions, hydraulic conductivity, and aquifer geometry. The second, contaminant and water level data, may consist of soil core data, aqueous concentrations, water and product levels in wells. Generally the second type of data is most abundant. The distinction between the two types of data is made because the first type of data correspond, even if roughly, to inputs to models and the second type to outputs from models.

Rarely are field data alone used in assessing a site. Some means are needed to extract information from the data. Usually this is done with models of various types. Models may take the form of simple formulas or complex numerical calculations. The simpler formulas and approaches may not be perceived as models, but they share similar characteristics. Each is based upon a set of assumptions which in some cases are well-matched by site conditions. Generally each also require ancillary data which are often obtained from the literature. In some cases these ancillary data are not easily obtained. The purpose of the methods and models described in this report provide a basis for evaluating field observations and extracting information from a variety of field observations.

The On-line Calculators

Each of the methods and models described in this document are available as a set of on-line calculators. They may be found on the Internet[1] at:

http://www.epa.gov/athens/onsite

The calculators were developed from interactions with state environmental agencies. The most important collaborations have been with the Region 2 Office of the New York State Department of Environmental Conservation and the Pennsylvania Land Recycling program[2].

Four types of calculations are found on the web site:

---

[1]Use of the calculators require that Javascript be enabled and that the Java 2 plug-in be available. See http://www.java.com/en/download/windows_automatic.jsp for more information.

[2]Other significant interactions have occurred with the North Carolina Department of Natural Resources, Ohio Bureau of Underground Storage Tank Regulations, Delaware Department of Natural Resources and Environmental Control, Wisconsin Department of Natural Resources , EPA Regions 9 and 4.

- formulas,
- models,
- scientific demos, and
- unit conversions.

The formulas generally represent inputs to transport models that are derived from field observations, literature data, or a combination of the two. These address concepts of field data assessment discussed in the Introduction. The models are intended to transfer knowledge gained from working on various sites. Because of limitations inherent to use of the Internet, it is not desirable to reproduce complex models as web applications. Primarily the ability to store data is severely restricted. The models are thus simple, but intended to introduce important concepts, rather than serve as competitors to PC models. The term "calculator" also represents the models, because they are intermediate between a hand calculation and a complex modeling application.

Two of the models have been selected for highlighting in this report. These appear in Chapters 2 and 3. The first model addresses the diving of contaminant plumes into aquifers. This behavior may be caused by recharge of rainwater. In light of the uncertainties in model parameters, this calculation is not expected to give some sort of exact answer, but is intended to be used to place well screens in the best possible vertical positions.

The second of the models is called "ConcentrationUncertainty" because it addresses the ranges of possible model behavior given uncertainty in model input parameters. As will be described, each parameter of the model is subject to some amount of uncertainty and this application highlights that uncertainty. To move beyond simply identifying this problem, the model can also determine generic parameter sets that always produce the worst (or best) case results. For some applications, single model runs with these parameters could be used for more certain decision-making, than the typical average parameter values used by modelers.

The remainder of the document (Chapter 4) is devoted to describing specific inputs to models, focusing on those that drive transport. Each of these calculations is described, along with literature and other input data. For each method an examination of typical results is given. For reference, Appendix 1 gives the Internet addresses for each calculator described in the text.

2. Plume Diving

This chapter describes the first of two models and its approach to their site-specific usage. The first model was designed to aid in the placement of monitoring wells by assessing the contribution of aquifer recharge to the vertical position of contaminant plumes. This topic will introduced through data from a site and three on-line tools. The on-line tools allow exploration of the apparent concentrations in boreholes that result from screen length and well placement choices[3], the estimation of vertical gradients from nested wells[4], and the approximation of vertical displacement of plumes due to aquifer recharge.[5] The first two of these calculators introduce the issues of vertical transport and the third allows site-specific data to be used for estimating plume diving and subsequent placement of well screens.

Vertical Delineation and Transport of Contaminants

Primarily contaminants are transported by flowing ground water. Thus the direction that the contaminant takes is determined by the direction of the flowing ground water. When ground water moves deeper into an aquifer, the contaminants are also transported deeper or "dive". This has an implication for sampling and well construction: the sample intervals must be located appropriately or diving plumes might be missed.

Data from the East Patchogue, New York gasoline release site (Weaver et al., 1996) are used to illustrate the consequences of ill-placed well screens. At this site there was an intensive characterization using vertically-discrete samplers. As a result the vertical distribution of contaminants is well-known. The second example is derived from this data and allows placement of well screens of differing lengths at differing depths in the aquifer. By encapsulating this idea in an applet, the implications of screen length and position can be seen directly from a data set.

These examples illustrate problems that can be created by inappropriate sampling locations. A simple calculation may assist in estimating the required placement of monitoring wells when recharge dominates vertical flow. This calculation is available in a calculator that is described below.

---

[3]The Average Borehole Concentration calculator: http://www.epa.gov/athens/learn2model/part-two/onsite/abc.htm.

[4]The Vertical Gradient calculator: http://www.epa.gov/athens/learn2model/part-two/onsite/vgradient.htm.

[5]The Plume Diving calculator: http://www.epa.gov/athens/learn2model/part-two/onsite/diving.htm.

1) East Patchogue, New York Plume Diving

The gasoline release at East Patchogue, New York created large BTEX and MTBE plumes (Weaver et al., 1996).   The plumes were detected when a private water supply well was constructed, used for a short time period, and then found to be contaminated. This well was located 4000 feet downgradient from the source. The well screen was about 50 feet below the water table, right where much of the MTBE mass was located.   The site investigation started at this point and went upgradient to identify the source.   Because of the importance of the aquifer for drinking water supply, the State of New York undertook an extensive investigation of the site which included vertical characterization of the plumes.   Multilevel samplers with 6 inch screens on five foot intervals were used.   The resulting vertical section through the plume showed that BTEX and MTBE tended to dive into the aquifer with distance from the source (Figure 1). Further, it was noted that a significant amount of diving occurred as the BTEX plumes passed under a gravel pit. By studying the well logs and performing a detailed hydraulic characterization of the aquifer with a borehole flowmeter, vertical migration controlled by stratigraphy was ruled out because the hydraulic conductivities varied by less than a factor of two over the aquifer. This left recharge as the most likely explanation for the plume diving. The model described in the sidebar was used to simulate the site and provided additional evidence for recharge as the cause of the diving.

The focus in this example is on how recharge pushes the plume downward, but water also discharges from aquifers.   Where water comes up at discharge points, so will the contaminants. This can happen along streams and rivers, at lakes, or the ocean.   The latter is the expected destination of the MTBE plume at East Patchogue. The ground water flow system discharges into Great South Bay adjacent to the southern shore of Long Island and ground water moves upward as it approaches its discharge point in the bottom of the Bay.
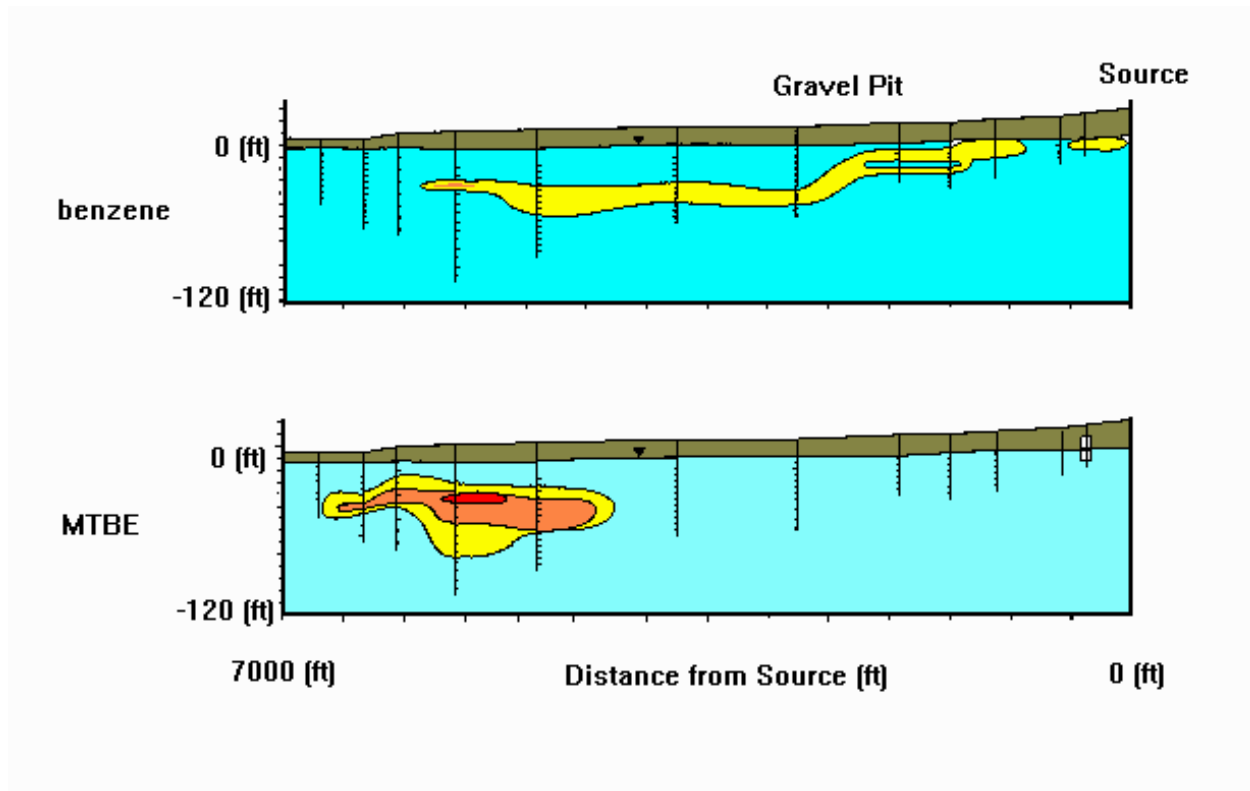
Figure 1 Vertical cross section through the MTBE, and benzene plumes. The gasoline source is located at the right hand edge of the sections and flow is to the left. Each of the plumes dives into the aquifer with transport in the aquifer.

Consequences

What about the consequences of plume diving, or more to the point, the consequences of missing a diving plume? The East Patchogue data set can be averaged to show what the plume would appear to be like if sampled only from long-screened wells. The data were averaged over the top ten feet of the aquifer to simulate twenty foot well screens "10 feet in and 10 feet out" of the aquifer. The data are plotted in Figure 2. This figure shows the maximum concentrations of MTBE, benzene and total xylenes along the length of the plume. These concentrations were the highest measured in the plume. Also plotted are the averages from the top ten feet of the aquifer. In this case the MTBE concentrations all fall below the State's threshold of 10 ug/L. With only these data we would have concluded that there was no MTBE plume at this site. Interestingly, the effect on benzene and total xylenes are that their plumes become the same length. The separation we expect to occur because of the differing tendency for sorption of benzene and xylenes has been negated by the sampling strategy. The total xylenes plume itself has not been shortened, because its length just reached the distance where diving would cause the plume to drop below the bottom of the monitoring wells. Benzene, however, did drop out of the monitoring network, and the simulated 10 foot long monitoring wells made the plume appear to be about one-third of its actual length.

5
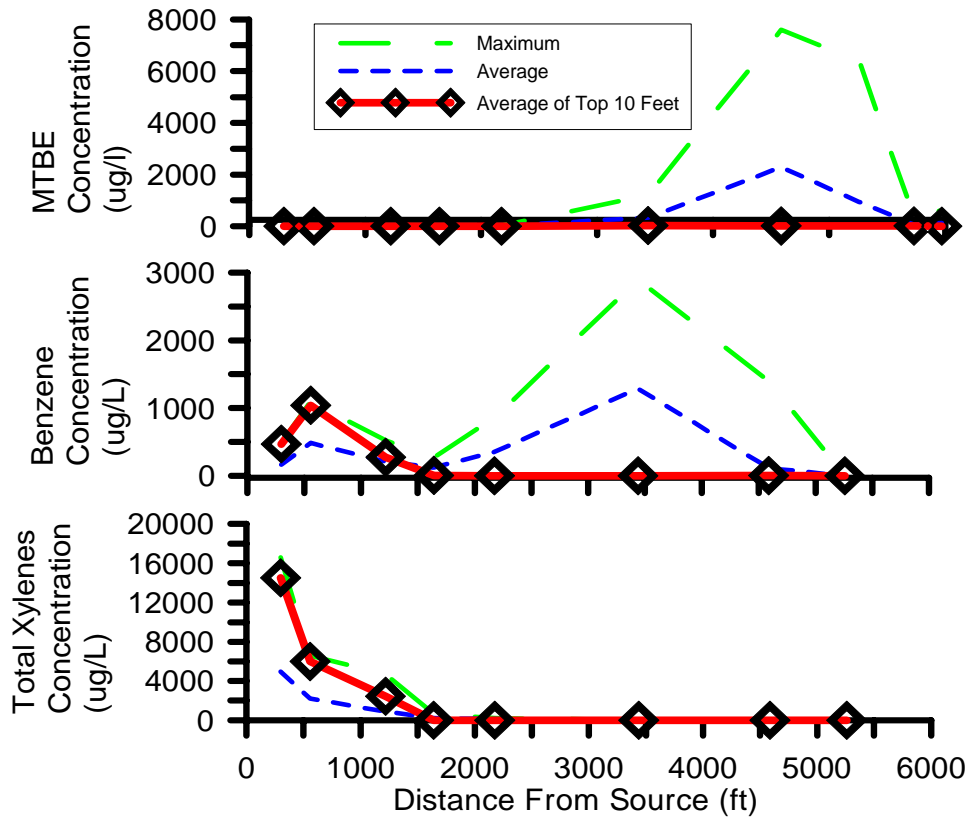
Figure 2 Consequences of sampling only the top ten feet of the aquifer at East Patchogue, New York. The MTBE plume would disappear (top); the benzene plume would be shortened by two thirds; and the total xylenes plume appears at the same length because its extent did not reach the gravel pit where diving dominates the contaminant distribution.

2) Average Borehole Concentration Calculator

The Average Borehole Concentration calculator demonstrates borehole dilution in screened wells. Borehole dilution occurs for at least two reasons: the placement of the screen relative to the contaminant and hydraulic conductivity distributions, and the length of the screen. The distribution of hydraulic conductivity and the vertical distribution of the contaminant are required for calculating the expected dilution. Since both of these are not commonly collected, the calculator has an embedded example. With these the user can see the effect of borehole dilution in hypothetical screened wells.

6
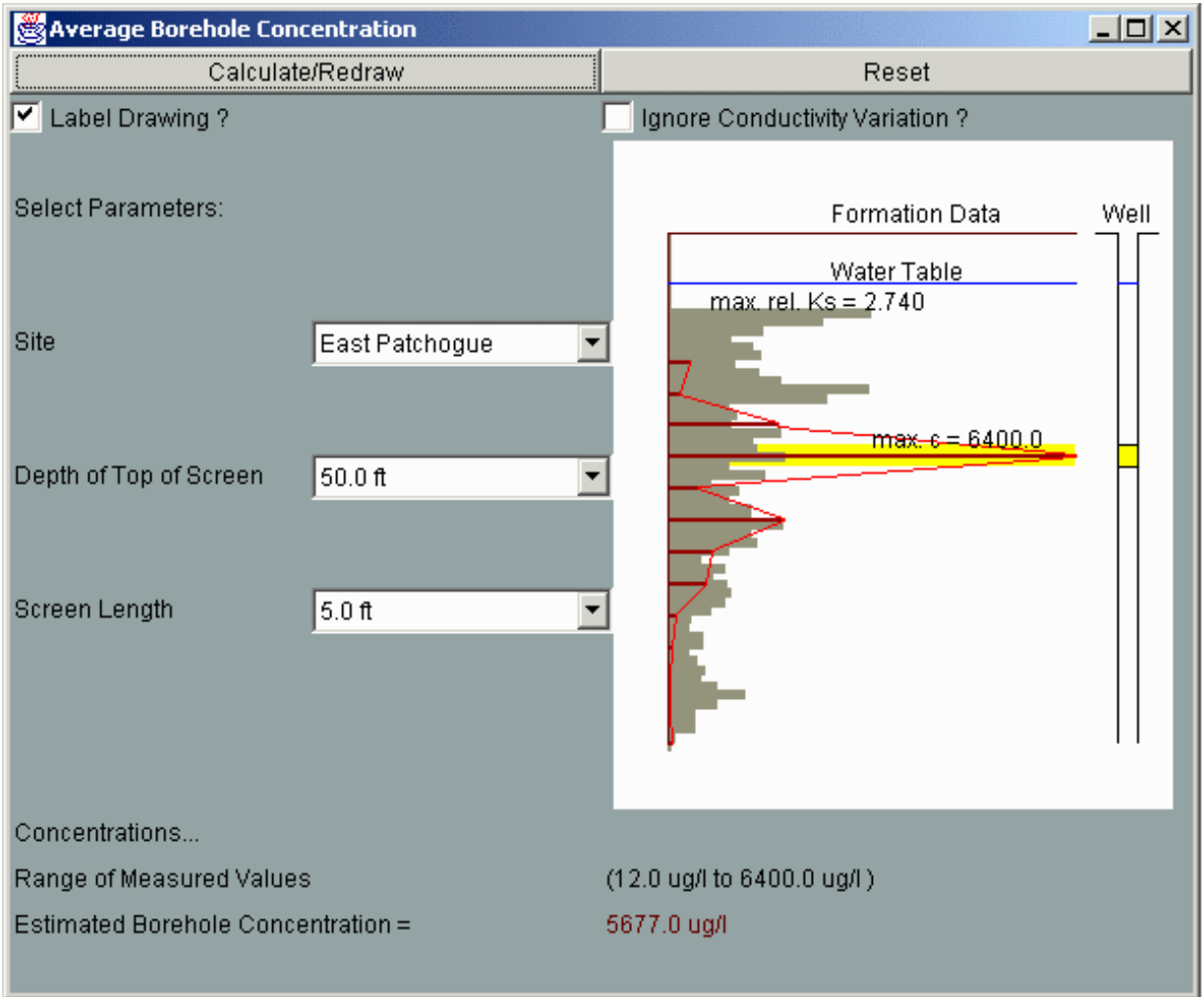
Figure 3 Average borehole concentration calculation.

The Embedded Data

The distribution of flow in the aquifer is represented by the relative hydraulic conductivies over the thickness of the aquifer. These data were collected from a borehole flowmeter on 1 foot to 3 foot intervals. Figure 4, part A, shows the distribution of hydraulic conductivity for a well at East Patchogue. Concentration data can be collected from a variety of vertical profiling methods. Each of these has a sampling interval that generally does not provide continuous coverage of the aqufier. In this illustration the sampling interval was 6 inches (Figure 4, part B). Between the actual sampling points, the calculator assumes linear variation of concentration. The user has the opportunity to select a screen depth and length (Figure 4, part C). With these the average borehole concentration that *would* have been seen in this well is calculated from the flow and concentration distributions. The users select the site, with its embedded data set, the depth of the top of the screen and the screen length.
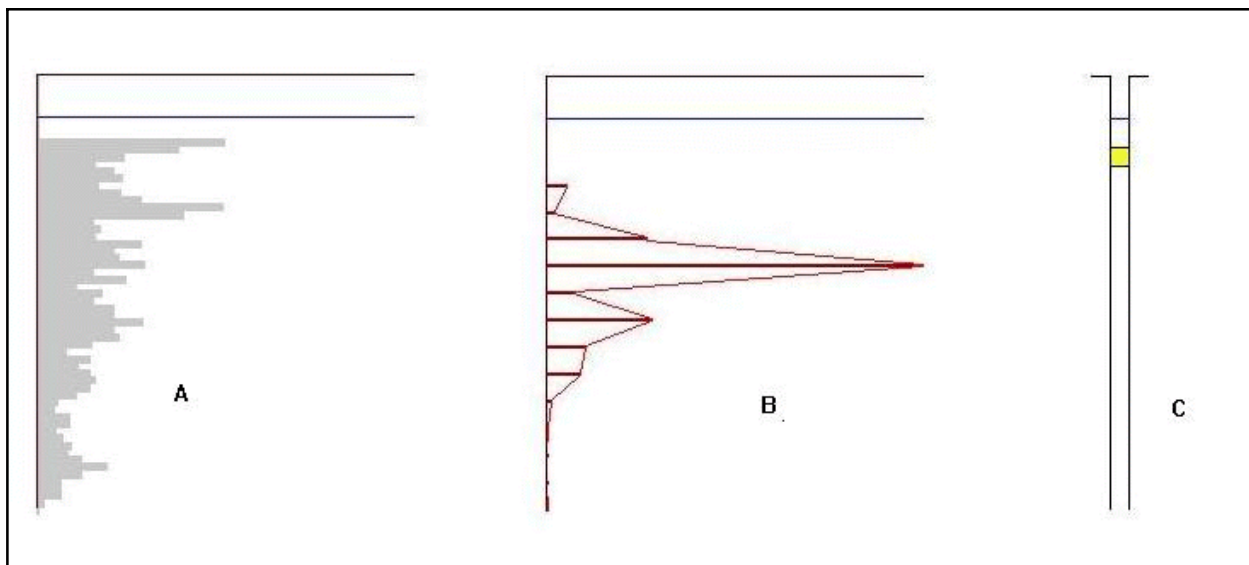
Figure 4 Illustration of components of borehole flow calculator graphics. "A" represents the distribution of hydraulic conductivity as measured by the borehole flow meter. "B" represents the distribution of concentration as measured at discrete sampling points. These correspond to the horizontal bars. The measured sampling points are connected by the diagonal lines. "C" represents the well with a screened interval indicated at some depth below the watertable.

The user may turn off the labeling of the drawing.   Labels may fall on top of drawing features of interest and this option removes the labels. The calculation may also be performed with the hydraulic conductivity variation ignored. Running the calculation with both options shows how much influence hydraulic conductivity variation has on the results.

Calculation Method

The average borehole concentration is calculated by averaging the mass flux from each layer in the profile. Each increment of mass flux is determined from

$$\Delta J_i \;\; = \;\; K_{ri} \int_{z_i^-}^{z_i^+} c(z)\, \Delta \tag{1}$$

where ΔJ_i is the increment of mass flux for depth increment i, K_{ri} is the relative hydraulic conductivity for the increment, $c(z)$ is the depth varying concentration over the increment, and z_{i-} and z_{i+} are the depths of the top and bottom of depth increment Δ, respectively. The integration is completed by assuming that $c(z)$ follows a linear function between the measurement intervals.

Example Results

The calculator provides a graphic which shows the superimposed distributions of hydraulic conductivity, the concentration distribution and an assumed screened monitoring well (Figures 3 and 4). The screened interval is indicated by a bar drawn over the data that originates in the well (Figure 4, part C). The bottom of the screen gives the results from the calculation along with the range of measured concentrations. Here (Figure 3) the concentrations measured from six-inch screens range from12.0 µg/l to 6400.0 µg/l. The five-foot long screened interval was placed 50 feet below the water table and had an expected concentration of 5677 µg/l. Because of the fortuitous placement of the well screen near the location of maximum concentration, the expected concentration is not off by much.

The expected concentrations differ with varying depth and screen length. The concentrations for a 20 foot screen located at 20 feet, 5 foot screen at 50 feet and and 10 foot screen at 70 feet below the water table are 120 µg/l, 5677 µg/l, and 994.7 µg/l, respectively. Figures 5 to 7 illustrate the well configurations for these examples.

With the top of the screen at 50 feet below land surface, well screens with length of 5 feet, 10 feet and 20 feet would give concentrations of 5677 µg/l, 4849 µg/l, and 3028 µg/l, respectively (Table 1). Thus the effect of increasing the screen length at this depth is to reduce the apparent concentration by one-half. When the screen is at 50 feet, the five-foot screen spans the point with highest concentration. Increasing the screen length includes depths that only have lower concentrations. The resulting ratio of concentration measured from a 20 foot screen to that measured from a five-foot screen is about 0.5 (given in the last row of Table 1). At other depths, say 40 feet, increasing the well screen length causes depths with higher concentrations to be included. In this case, the apparent concentration increases with screen length. Thus, varying the screen length may increase or decrease the apparent concentration depending upon its placement relative to the underlying contaminant distribution. When the ratio in Table 1 is less than one, increasing the screen length decreases concentration and vice versa. In these examples there are as many cases with the screen length increases the apparent concentration as that decrease it.

9

Screen Length (feet)	Depth of Well Screen Top							
	20 feet	30 feet	40 feet	50 feet	60 feet	70 feet	80 feet	90 feet
5	0	280	1054	5677	877	1155	561	80
10	0	210	1805	4849	1054	995	476	62
20	120	761	3524	3028	1130	743	316	37
Concentration ratio (20 ft screen:5 ft screen)								
	– –	2.7	3.3	0.53	1.3	0.64	0.56	0.46

Table 1 Effects of well screen length on concentrations given in µg/L observed wells screened from 20 feet to 90 feet below the land surface at East Patchogue, New York.
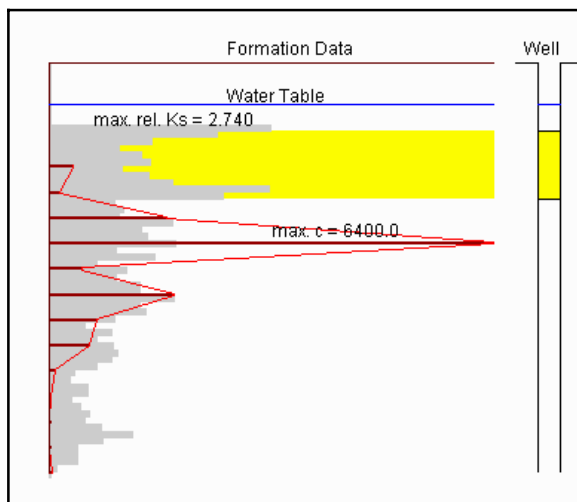
Figure 5 Estimated borehole concentration of 120 µg/L for a twenty-foot long well screen located 20 feet below the land surface.
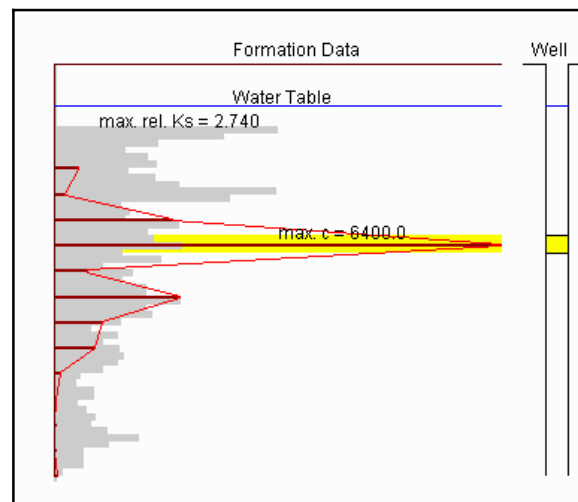
Figure 6 Estimated borehole concentration of 5677 µg/L for a five-foot well screen located 50 feet below the land surface.
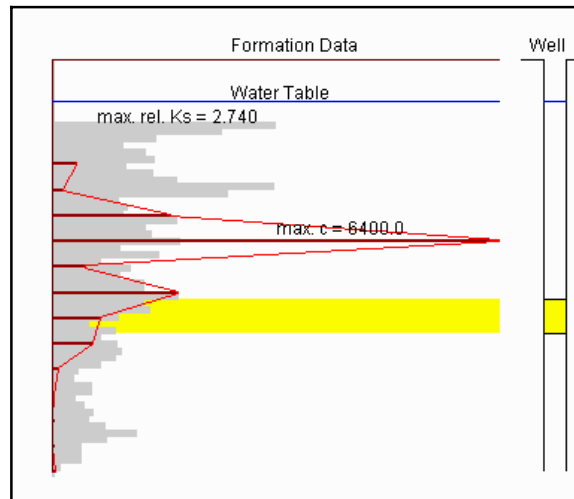
Figure 7 Estimated borehole concentration
of 995 µg/L for a ten-foot long well screen
placed 70 feet below the land surface.

3) Observation of Vertical Gradients

Estimation of vertical gradient are one tool for assessing the possibility of vertical flows. Water levels in nested well clusters (wells located closely together) indicate upward or downward flowin aquifers or flow between adjacent geologic units. Flow is governed by Darcy's Law:

$$q = -K \frac{Change\ of\ head}{Distance} \tag{2}$$

where q is the Darcy flux (volume of water per unit area per unit time) [L/T] and K is the hydraulic conductivity [L/T]. The change of head (roughly water level) divided by the distance determines the magnitude and direction of flow. Figure 8 shows the relative relationships between two wells. With respect to each other, one is shallow and the other deep. The figure also indicates the important dimensions: depth to water (dw), depth to the top of the screen (d) and the screen length(s).
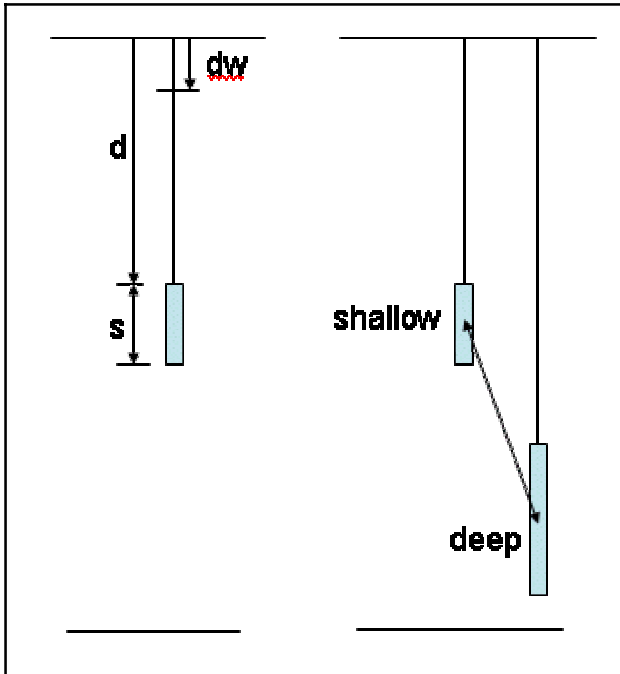
Figure 8 Definition of relationships for vertical gradient calculations: dw is the depth to water, d the depth to the top of the well screen, and s is the screen length. In relation to each other one well is shallow and the other deep.
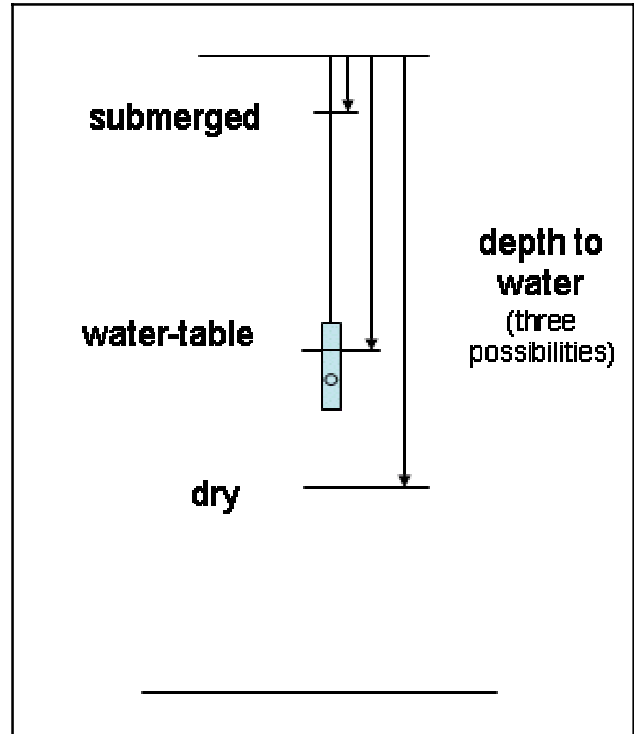
Figure 9 Submerged, water table and dry conditions of a well screen.

One choice for calculating the gradient is to use the mid-points for determining the distance in the denominator of equation 2 (as illustrated in Figure 8). In performing the calculation there are three possibilities for how the water levels relate to the well screen (Figure 9):

- *Submerged*. The water level is above the top of the well screen.
- *Water-table*. The well screen intersects the water-table. The gradient is calculated from the mid-point of the water level and the bottom of the well screen.
- *Dry*. The well is dry and no calculation is performed.

Theoretically, the gradients are determined from piezometers that are only open at the bottom and thus have an effective screen length of zero. In practice, since wells with screens of various lengths are used to calculate the gradients, the screen lengths may have an influence on the calculated gradients.

12
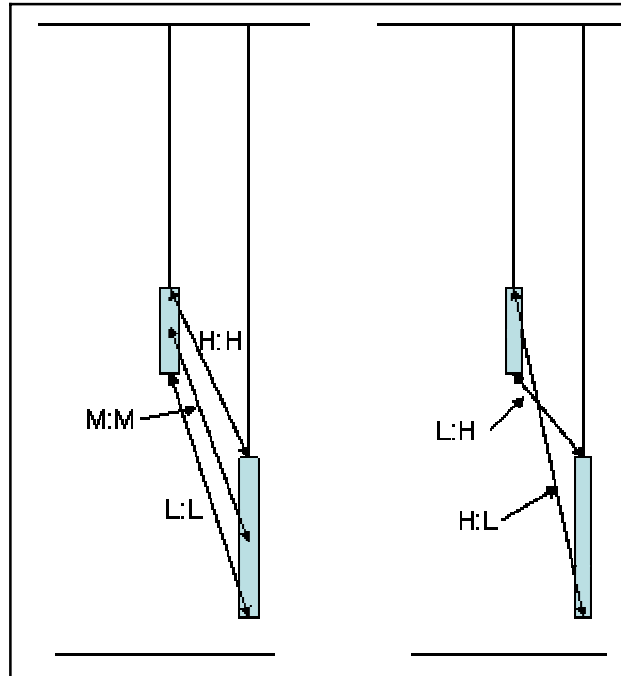
Figure 10 Assumed distances for vertical gradient calculation: H = high, M=medium, L=low.

Five choices are made concerning screen lengths and are illustrated in Figure 10:

- Distance is from top of screen to top of screen (H:H)
- Distance is from mid-point of screen to mid-point of screen (M:M)
- Distance is from bottom of screen to bottom of screen (L:L)
- Distance is from top of screen to bottom of screen (H:L)
- Distance is from bottom of screen to top of screen (L:H)

For screens of equal length the first three choices all give the same result, no matter the relative depth of the screens. In addition they give the same value as a piezometer open at the midpoint depth of the screen. By supplying results for all these possibilities, a range of values is provided that would bracket the "true" value of the gradient.

The previous discussion presumes that the well is screened in a uniform or fairly uniform material. To avoid complexities of heterogeneity, this placement is desirable. Figure 11 illustrates the difficulty when different materials are present. Here sand is assumed to overly a tight clay. If there was an upward gradient, the head in the clay would be higher than the head in the sand. The upward gradient might be best represented by assuming that the head in the well represented a point at the bottom of the screen rather than the top where the sand exists.

13
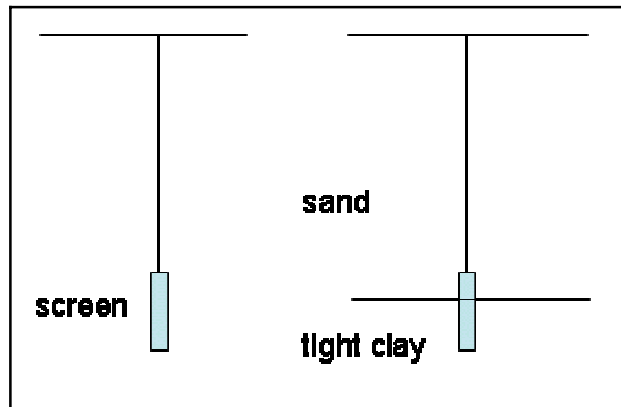
Figure 11 Gradients in wells that are screened in heterogeneous materials.

Well Cluster Example

Data from a field site in Michigan are shown in Table 2. The site had three closely-spaced wells with screens located at different depths. The wells were intended to serve a cluster and were placed as close together as practical. These were used to generate the gradient estimates that are summarized in Table 3. For the first pair of wells (W-404S and W-405M) the gradients are directed downward for all estimates and range in magnitude from 0.0057 to 0.016, a difference of 65%. The midpoint to midpoint estimate of 0.0083 is close to the assumed piezometer value of 0.0068. The difference between the two is due to the different screen lengths in the two wells.

Flow is upward between the second pair of wells (W-405M and W-406D) and varies by 26%. The values are lower by a factor of ten, reflecting the smaller difference in depth to water than for the first pair. Since the screen lengths are the same for these two wells, the piezometer and midpoint estimates are the same.

Well	Elevation of Top of Casing (ft)	Depth to Water (ft)	Screened Interval (ft)
W-404S	626.44	9.10	7.6 - 17.6
W-405M	626.73	9.51	25.6 - 30.6
W-406D	626.77	9.54	40.2 - 45.2

Table 2 Example field data for vertical gradient determination.

Wells	Estimated Gradients				
	direction	Smallest	Midpoint to Midpoint	Piezometer	High Value
W-404S & W-405M	down	0.0057	0.0083	0.0068	0.016
W-405M & W-406D	up	0.00051	0.00069	0.00069	0.0010

Table 3 Example gradient estimates indicating the smallest, midpoint to midpoint, highest and the value for a piezometer.

Application to Plume Diving

At the East Patchogue field site, the average annual recharge rate was estimated to be 22 in/yr. This value, coupled with an estimated hydraulic conductivity of 400 ft/d, can be used to estimate a bounding vertical gradient. If all the recharge water moved only vertically in the aquifer, the maximum gradient would be 0.0000125 ft/ft.[6] Could this gradient be observed in monitoring wells?

Vertical Distance between Screens (ft)	Gradient Magnitude (ft/ft)
10	0.001
20	0.0005
100	0.0001
1000	0.00001

Table 4   Gradient magnitude for a difference in head of 0.01 ft and various distances between well screens.

The gradient is determined from the difference in water elevation and the distance between the measuring points (Equation 2).   Here the difference in water elevation could be

---

[6]The gradient was calculated from 22 in/yr (0.005 ft/d) divided by 400 ft/d.

assumed to be the smallest measurable difference: 0.01 feet. By selecting various distances between the screens, Table 4 shows that a difference of 1000 ft in screen position is necessary to detect a vertical gradient of 0.00001. Thus it is unlikely that recharge-driven plume diving would be detected by water level differences in monitoring wells.

Recharge-Driven Plume Diving Calculation

The prospects for plume diving should be considered when placing wells at *all* sites. The first consideration should be indications of dipping strata from well logs. These can control the distribution of contaminants down gradient from the source. Recharge can also cause plume diving. The calculator shows the effect due to recharge only. The implication of the results are that for some aquifers the recharge of clean water to the aquifer can push the plume deeper into the aquifer.

The plume diving calculator was designed to be used as a tool for site assessment by following these steps:

- Estimate the required parameters for the each segment of the flow system:
    - Up and down gradient heads,
    - Aquifer hydraulic conductivity, and the
    - Recharge rate.
- Run the calculator for the proposed well location,
- Check the plume depth at the location, and
- Locate the well screen in appropriate vertical intervals.

The calculator (see Figure 12) uses a simple aquifer model, in complex geological settings a more complex model would be required to show the effects of recharge on plumes.
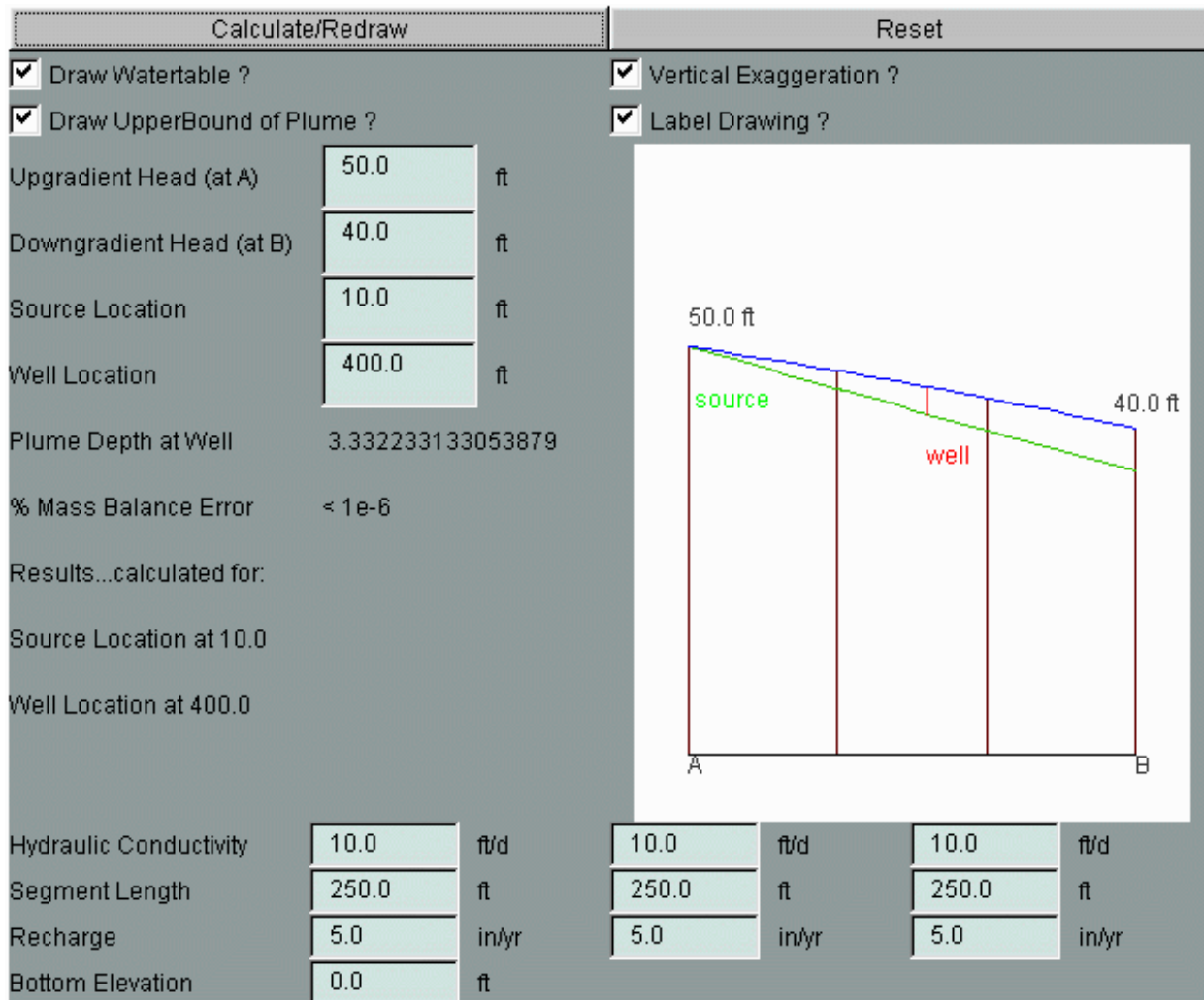
Figure 12 Input and output screen for the plume diving calculator.

Theory

The recharge calculator is based upon two solutions of the one-dimensional Dupuit equation for flow in unconfined aquifers. These solutions are combined to determine the position of the phreatic surface (water table) and a streamline originating at the water table, the gradient, ground water fluxes and travel times for sorbing contaminants. The methods used for performing these calculations are given in Appendix 3.

East Patchogue Example

This method was developed for application to the MTBE and benzene plumes at East Patchogue, New York. At this site the plume appeared to drop when it moved below a sand and gravel mining operation. Data collected from a borehole flow meter on the variation of hydraulic conductivity with depth showed no direct connection between contaminant concentrations and hydraulic conductivity. From this it was concluded that statigraphy did not cause the diving of the plume. The plume diving calculation was developed to assess the contribution of recharge to the dropping of the plume. The results of the calculations are shown in Figure 13. The line labeled "A" represents the water table, which was calibrated to observed elevations.   The line labeled "B" was determined from the plume diving calculator, using the calibrated water levels, hydraulic conductivity calibrated from a transport model (Weaver, 1996), and assumptions concerning the recharge. Most importantly, the average recharge on Long Island is estimated to be 22 in/year by the USGS. In the area of the sand and gravel pit (Segment 2 on Figure 13) the entire annual rainfall of 44 in/year was assumed to recharge the aquifer. The combination of these inputs was sufficient to produce line "B" which is the best estimate of the upper bound of the contaminant plume.

Although the calculation reproduces the field behavior, the best use of the calculator is where vertical data are not yet available. Using recharge estimates and land use characteristics an estimate of plume diving can be made. Sampling can then be made at appropriate elevations. Since there are many factors that influence the accuracy of the method, not the least being the assumption of one-dimensional flow, the calculator predictions are not intended to give the "last word" on plume diving. Rather the calculator results should guide placement of well screens.
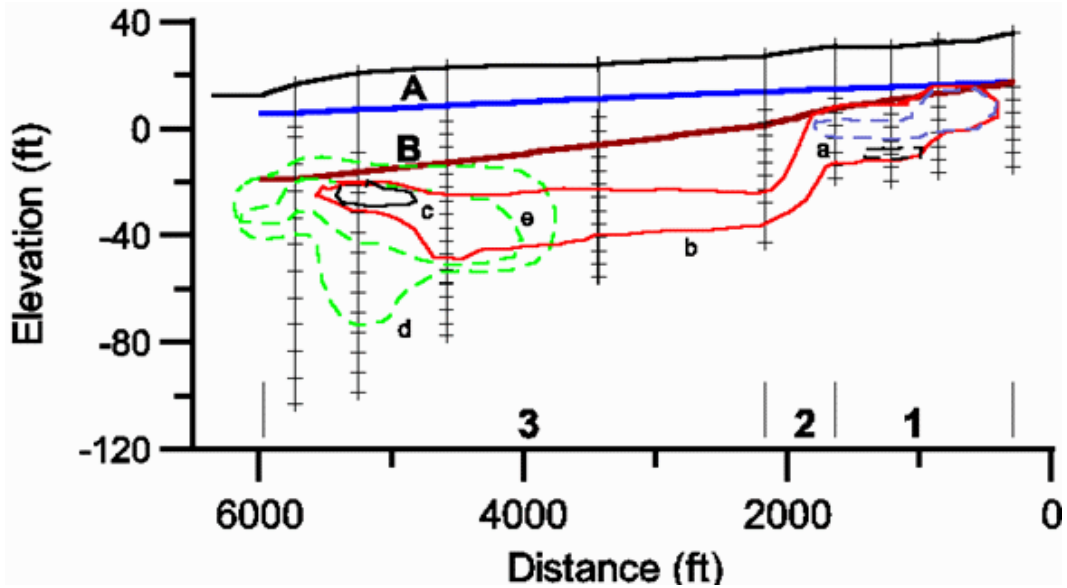
Figure 13 Example plume diving calculation for the East Patchogue site. "A" represents the watertable which was calibrated to the field data. "B" represents an uncalibrated prediction of the top of the plume determined from the plume diving calculator.

Required Input

The plume diving calculator requires input to 1) Define the hydraulics of the flow system and 2) Contaminant source and observation well location. The single screen of the plume diving interface is used for parameter entry, reporting of results and graphing the solution. The following drawings show an exploded view of the interface.

Flow System Hydraulics

The aquifer is divided into segments and for each the hydraulic conductivity, recharge rate, and length must be specified (Figure 14). A uniform aquifer can be simulated by using the same parameter values for each segment.

	Segment 1		Segment 2		Segment 3	
Hydraulic Conductivity	10.0	ft/d	10.0	ft/d	10.0	ft/d
Segment Length	250.0	ft	250.0	ft	250.0	ft
Recharge	5.0	in/yr	5.0	in/yr	5.0	in/yr

Figure 14 Plume Diving calculator hydraulic and hydrologic property entry.

19

Source and Observation Well Locations

Two heads are specified, one for the upgradient end of the flow domain at point (A) and one at the downgradient end (B).   Within this domain, the locations for the source of contaminants and the well are then entered on the side panel (Figure 15).

Upgradient Head (at A)	50.0	ft
Downgradient Head (at B)	40.0	ft
Source Location	10.0	ft
Well Location	400.0	ft

Figure 15 Plume Diving calculator location entry.

For a source that covers a large area (free product zone, landfill, etc.) the source location should be taken as the *down gradient edge* of the source.

The well location is used to show how much plume diving to expect at a point down gradient from the source (Figure 16). The well is indicated by a red line on the output that shows the difference between the water table and the top of the plume.
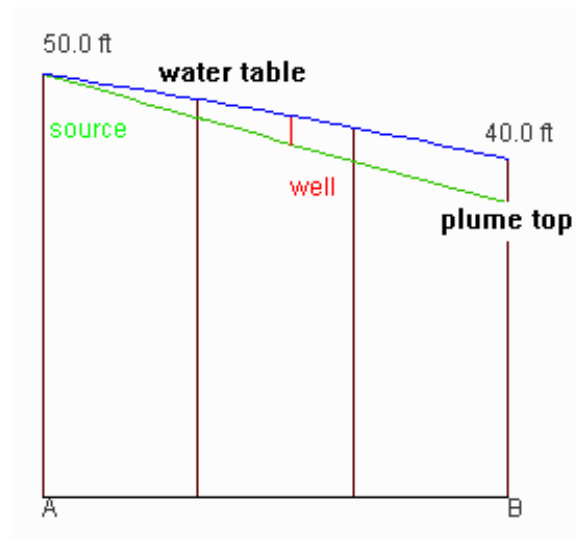
Figure 16 Plume Diving calculator graphical output.

Model Results

In addition to the graphical output, the depth *below* the water table is output, as is the over all mass balance error. The source and well locations are echoed in this section (Figure 17).


```
Plume Depth at Well        3.332233133053879

% Mass Balance Error      < 1e-6

Results...calculated for:

Source Location at 10.0

Well Location at 400.0
```

Figure 17 Plume Diving calculator mass balance output.

Drawing Options

The features graphed on the drawing can be customized by (Figure 18)

- Labeling
- Drawing the water table
- Drawing the top (upper bound) of the plume
- Vertically exaggerating the drawing


```
☑ Draw Watertable ?              ☑ Vertical Exaggeration ?
☑ Draw UpperBound of Plume ?     ☑ Label Drawing ?
```

Figure 18 Plume Diving calculator display options.

Drawing the top (upper bound) of the plume automatically turns on drawing of the water table. When vertical exaggeration is turned off, the horizontal and vertical scales of the drawing are the same.

3 Contaminant Transport

When confronted with the possibility of contaminated ground water, questions often asked by the public include:

- Will my well become contaminated?
- When will contaminants reach my drinking water supply?
- How bad will it be? (i.e., How high will the contaminant level be?)
- What are the effects of drinking this water on my children or myself?

The ability to answer these questions presumes a predictive capability that cannot be achieved by monitoring alone. Thus many agencies and individuals turn to models to provide answers to these questions.   Models are chosen for this task because

- they have an evident ability to predict future concentrations,
- they have a scientific basis,
- they have the ability to include the effects of many different factors, and
- they have become accepted as predictive tools.

A number of factors, however, influence and limit the ability of models to predict future contamination. The proper usage of models depends on the details of their construction and how they are used for a specific problem. As will be seen to be the major thrust in the following section, an accounting for uncertainty should be included as a part of model usage.   A calculator called the ConcentrationUncertainty calculator[7] will be used to show the impacts of parameter variation on contaminant transport and the generation of generic worst-case parameter sets.

First Arrival Versus Advective Travel Times

Before beginning the discussion on model application, several concepts in subsurface transport are introduced in this section.

Frequently the advective travel time is used as a rough guide for contaminant transport. If contaminants were transported only by movement with the ground water, then the travel time from a source to a receptor would be the advective travel time.   Figure 19 shows a schematic illustration of transport by advection only compared against transport by advection and dispersion.

---

[7]The ConcentrationUncertainty calculator can be found at http://www.epa.gov/athens/learn2model/part-two/onsite/uncertainty.htm
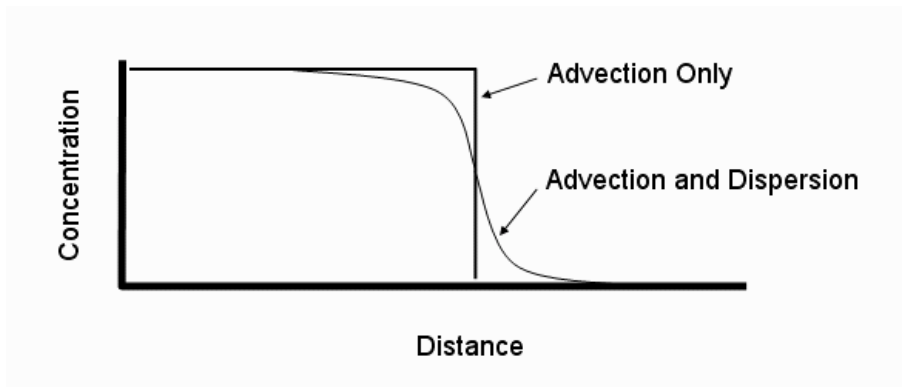
Figure 19 Illustration of transport by advection only (hypothetical) and transport by advection and dispersion.

The advective travel time, $t_{advective}$, is calculated from Darcy's Law and a retardation factor:

$$t_{advective} \quad = \quad \frac{x_{receptor}}{v_s / R} \tag{3}$$

where $x_{receptor}$ is the distance to a receptor in the aquifer (i.e., a well) [L], R is the retardation factor [dimensionless], and v_s is the seepage velocity [L/T]. The retardation factor is the ratio of transport velocities of a conservative tracer to that of a sorbing chemical. The seepage velocity is defined from Darcy's Law:

$$v_s \quad = \quad \frac{v_d}{\theta} \quad = \quad \frac{-Ki}{\theta} \tag{4}$$

where v_d is the Darcy flux [L/T], K is the hydraulic conductivity [L/T], i is the hydraulic gradient, and θ is given variously as the effective porosity or total porosity [L^3/L^3].

In contrast to this simple approach (Figure 19 and Equation 3), transport is also subject to dispersion[8] and biodegradation. Transport by advection alone does not occur in ground water because there is always some spreading of a sharp front (illustrated by the abrupt drop of concentration in the advection only case). At some time after a release, the contaminant arrives at a given location. Because of spreading caused by dispersion this time will be sooner than if only advection is included.

---

[8]Dispersion is properly interpreted as differential advection through materials of various hydraulic conductivity. Were this properly accounted in a simple formula as Equation 3, there would be less of a need for the approach that follows.

Advective travel time is an appealing quantity because of its conceptual and calculational simplicity.   But, the first arrival time of a contaminant can be calculated easily and can incorporate the threshold concentration of concern, biodegradation, dispersion, advection, retardation, source concentration and source lifetime. Figure 20 illustrates the first arrival time and other concepts to be applied in following calculation. Given a receptor located some distance from a contaminant source, no contamination is observed at the receptor when the release begins. Because of the distance some amount of time is required to transport the contaminant from the source to the receptor. In the Figure, this time period is about 1400 days. After that time, the contaminant concentration rises. The gradual rise occurs because subsurface transport occurs through a heterogeneous medium with different rates in different parts of the medium. The time when the contaminant first goes above the concentration of concern (CoC) is called the first arrival time. As more contamination arrives at the receptor, the concentration increases until a maximum is reached. This is called the maximum concentration.   The maximum concentration cannot exceed the source concentration and may be reduced much lower from dispersion or biodegradation. In the case shown in Figure 20, the maximum concentration does equal the source concentration. If the source of contaminant is finite, at some time the concentration at the receptor will decline and drop below the concentration of concern.   The time period that the concentration is above the level of concern is called the duration.

It is possible for dispersion and biodegradation to cause the contaminant concentration to be reduced to below a threshold level of concern before the chemical reaches a specified receptor. In this extreme case, the concept of advective travel time has no relevance to the receptor. In other, less extreme cases, contamination may rise above the level-of-concern sooner than the advective travel time, and a protection strategy based upon advective travel time is non-conservative.

The concentration of concern would normally be chosen as an maximum concentration level (MCL) or other value. For example the federal MCL for benzene is 5 µg/L. The US EPA Office of Water has given a drinking water advisory for MTBE at a level of 20 µg/L to 40 µg/L. These levels could be chosen as CoCs. The first arrival time, duration and maximum concentration all can vary from those shown in the Figure, depending upon the source and transport properties.
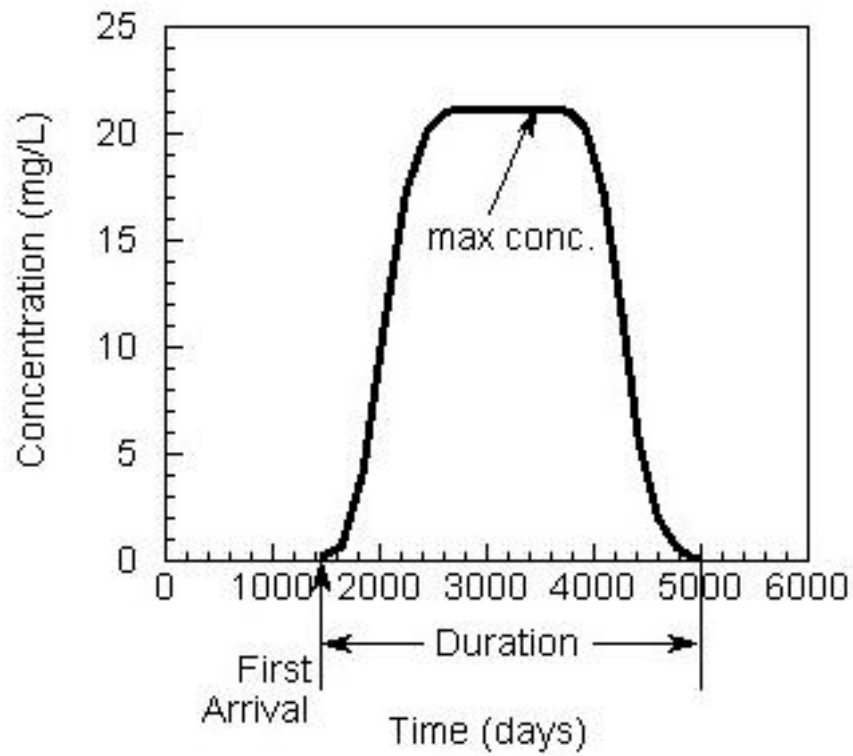
Figure 20 Illustration showing the relationship between the first arrival time, maximum concentration and duration of contamination. The first arrival time and duration are determined relative to a given threshold concentration, that is usually a maximum contaminant level or other concentration of concern.

Uncertainty Range Determination

Models are commonly viewed as useful tools for understanding contaminant transport (Oreskes et al., 1994) and determining future risk (ASTM, 1995). The degree of predictive capability of subsurface transport models has, in fact, not been established (e.g., Miller and Gray, 2002, Eggleston and Rojstaczer, 2000). Given that the values of all the parameters (hydraulic conductivity, dispersivity, retardation factor, biodegradation rate constant) and the forcing function (source concentration and source duration) were known, and that the assumptions behind the model were exactly met, the model equations (Equation 24) could be solved for the required outputs. In the real world, however, the values are not exactly known and no aquifer would meet the required assumption of homogeneity. At leaking underground storage tank (LUST) sites, it would typically be expected that hydraulic conductivities would be measured through slug tests and the other input parameters not measured. The source concentration and duration would be unknown. Dispersivity, since it represents unaccounted heterogeneity, is clearly not a fundamental parameter and is best viewed as a fitting parameter: thus its appropriate value is also unknown.

Models are more likely to provide a framework for understanding transport than for predicting future exposure and risk. Commonly, models are calibrated to field data to demonstrate their ability to reproduce contaminant behavior at a site. This process implies a degree of correctness in understanding and provides the first step toward demonstration of predictive ability. For screening sites or where rapid response is required, sufficient data may not be collected for calibrating a model. How then should models be used in situations where they can not or will not be calibrated? What are the plausible ranges of output given uncertainty in inputs? Can worst case parameter sets be selected that always provide a bound on plausible outcomes?

Figure 21 shows a conceptual relationship between uncertainty and data availability. With small amounts of either measured input data or calibration data, the resulting model uncertainty is high. Models may still be useful in these cases, but their uncertainty should be quantified so that their results are not taken falsely as inerrant.
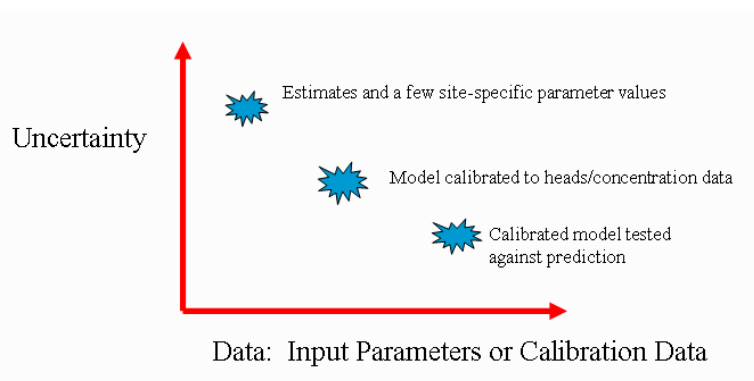
Figure 21 Relationship of uncertainty to model data availability.

26

Approach

Several approaches to uncertainty analysis have been developed. Generally these require knowledge of parameter values and their statistical distributions including correlations between individual parameters. Here site investigations are not sufficiently detailed to determine values for some of the parameters, let alone their statistical distributions and correlations.   A brief accounting of the model inputs is given as follows: Porosity and dispersivity are essentially never determined on a site-specific basis, despite their importance in determining model outcomes.   Biodegradation rate constants may be estimated from simple techniques (Buscheck and Alacantar, 1995), but these require adherence to a suite of restrictive assumptions that limits the results by the same considerations that we are attempting to address in this work. Parameters measured in the field are subject to uncertainty because of spatial variability (hydraulic conductivity and fraction organic carbon) or temporal fluctuations (gradients). The forcing parameters of the model, initial concentration and duration, are rarely known, because contamination is normally discovered years after a release occurs.

There is a similar lack of knowledge of statistical distributions of the inputs. A widely-used alternative is to assume knowledge of the statistical properties by using scientific literature values as substitutes. These approaches allow assignment of probabilities to the various outcomes, but suffers from obvious lack of site-specificity. Where results depend strongly on assumed distributions, it is not possible to determine how much error is introduced into the results from the distributions. Alternatively, if it is assumed only that plausible ranges of input parameters are known, similar outcomes can be determined, but probabilities cannot be assigned. Because of lack of knowledge of the underlying probability distributions, a method based on ranges of inputs was developed.

Nine parameters of the one-dimensional model (Equation 24) are assumed to be variable. Tables 5 and 6 list parameters and their treatment in the model. All seven parameters of the model were allowed to be variable, as were the concentration and duration of the source. The chemical, distance to receptor, and minimum concentration of concern are taken as fixed for a given analysis. With this selection of inputs there are two values each for nine parameters: the minimum value and the maximum value. This leads to a total of 2^9 or 512 unique combinations of parameters. This calculation highlights an assumption of this method: That each parameter value is equally likely and can occur in combination with each other parameter value. In other words that each parameter is uniformly distributed and uncorrelated.   The large number of parameter combinations is the reason to seek models that execute rapidly. Hence the interest in the one-dimensional model.

Figure 22 shows an example output where breakthrough curves representing various breakthrough curves have been plotted. These have been selected from the 512 outputs of the model to represent the significant outputs of the model: earliest and latest first arrival times, minimum and maximum peak concentration, and the longest and shortest duration.   Along with

these the breakthrough curve for the average values of the inputs was plotted. It's clear that a wide variety of breakthrough curves is possible from this model, given the selected input range.
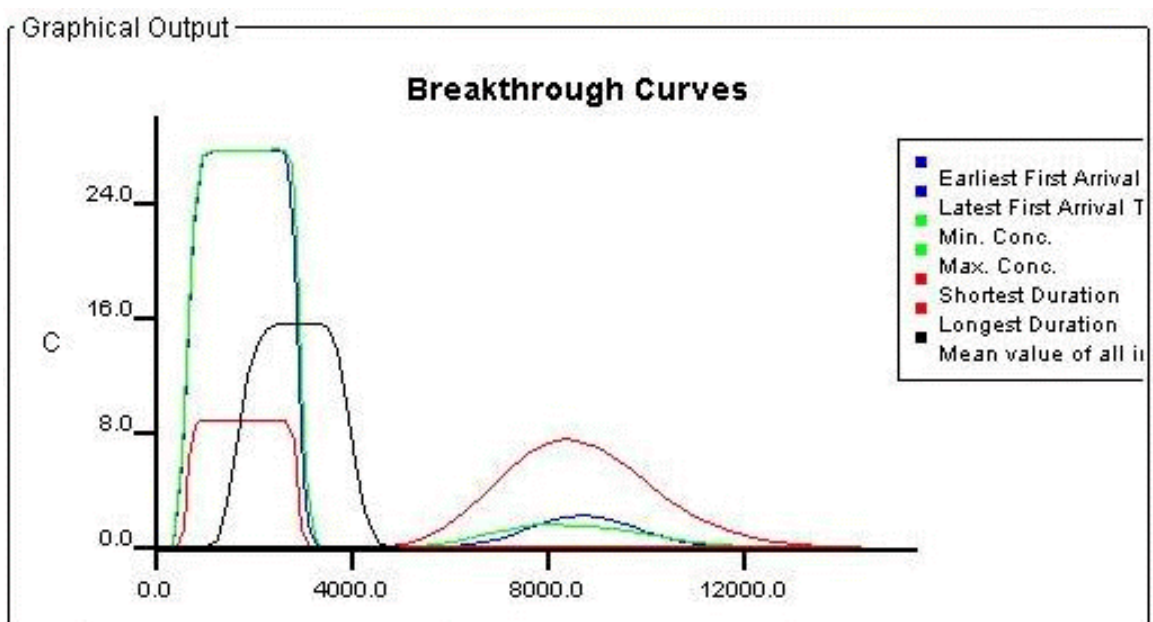
Figure 22 Output from the Concentration Uncertainty applet showing the wide range of breakthrough curves that are possible given specified ranges of input parameters. Concentrations in milligrams per liter are plotted against time in days.

Quantity	Treatment	Example Problem Values		
		Low		**High**
Model Parameters				
Hydraulic Conductivity	variable	Low Scenario	15 ft/d	50 ft/d
		High Scenario	108 ft/d	328 ft/d
Porosity	variable	0.20		0.25
Gradient	variable	0.001		0.005
Fraction Organic Carbon	variable	0.0001		0.001
Organic Carbon Partition Coefficient	variable	31 L/kg		106 L/kg
Dispersivity	variable	0.1 * estimate from Xu and Eckstein (1995)		10 * estimate from Xu and Eckstein (1995)
Half Life	variable	Low Scenario	100 days	730 days
		High Scenario	4000 days	6000 days

Table 5 Parameter inputs, their treatment in the model as fixed or variable and the values used in the model uncertainty example.

Quantity	Treatment	Example Problem Values		
		Low		**High**
Problem Definition				
Source Concentration	variable	10 mg/L		30 mg/L
Source Duration	variable	1500 days		3000 days
Chemical	fixed	benzene		benzene
Distance to receptor	fixed	Low Scenario	50 ft	50 ft
		High Scenario	500 ft	500 ft
Minimum Concentration of Concern	fixed	0.005 mg/L		0.005 mg/L

Table 6 The problem definition, its treatment in the model as fixed or variable and the values used in the uncertainty example.

Simulation

In order to compare various scenarios, four outputs are generated from the modeled breakthrough curves: 1) first arrival time, 2) maximum concentration, 3) duration of

contamination, and 4) risk factor.   This first three of these are illustrated in Figure 22. Cancer risk is normally determined from an expression of the form (US EPA, 1989)

$$Risk \quad = \quad I \; SF \quad = \quad \frac{CW \; ED \; EF \; IR}{BW \; AT} \; SF \tag{5}$$

where I is the intake in mg/kg-day, SF is the cancer slope factor (kg-day/mg), CW is the concentration in water (mg/L), ED is the exposure duration (days), EF is the exposure frequency (days/year), IR is the injestion rate (liters/day), BW is the body weight (kg), and AT is the averaging time (years).   Since concentrations on the breakthrough curve change with time, the effect of the transient in concentration is included in the risk equation by using the substitution:

$$CW \; ED \quad = \quad \int_{t_o}^{t_a} CW(t) \, dt \tag{6}$$

where CW(t) are the modeled concentrations, t_o is the contaminant first arrival time, t_a is the last time that the concentration is above the threshold. Thus the integral of concentration versus time gives a measure of relative risk. The model accumulates results and determines the best and worse cases for each of the four chosen breakthrough curve outputs.

In addition to variable parameters, four scenarios were created to simulate a variety of conditions and determine if the model behavior was similar despite variation in parameter values. Two ranges each of hydraulic conductivity and half life were selected (Table 6).   These variables were chosen to vary because they have a direct effect on model outputs: Hydraulic conductivity affects advective transport rates and thus the arrival times and duration of contamination, and the half life impacts maximum concentration. Risk is affected by both concentration and duration. The scenarios are generally comparable with each other with the exception that the receptor is closer to the source in the low conductivity scenario. This selection was made so that there would be complete breakthrough curves for all combinations of parameters in each scenario.

Results

Table 7 shows the extreme cases for four problem scenarios (see Table 5): High and low conductivity aquifers, and high and low biodegradation rates. These results show the magnitude of possible outcomes given the range of inputs used.   The high and low conductivity scenarios have a different distance to the receptor (500 ft versus 50 ft), so the first arrival time results are not directly comparable. In going 10 times further in the high conductivity scenario the arrival time is approximately 2.5 times greater than the low conductivity scenario (20 days/7.9 days), indicating proportionately earlier first arrival in the high conductivity scenario.   The minimum durations are in part determined by the source duration (which at a minimum is 1500 days). With high biodegradation rates the minimum concentrations can be greatly reduced (compare row a and b and row c and d in column 3) in either scenario.

30

	First Arrival Time (days)		Maximum Concentration (mg/l)		Duration (days)		Risk Factor (day-mg/l)	
	Earliest (1)	Latest (2)	Lowest (3)	Highest (4)	Shortest (5)	Highest (6)	Best (7)	Worse (8)
High Conductivity Scenario (receptor located 500 feet from the source)								
(a) Low Biodegradation	20	1140	6.4	30	1580	8310	2.01e5	1.95e6
(b) High Biodegradation	20	1760	0.0081	28.3	1340	7210	562	1.54e6
Low Conductivity Scenario (receptor located 50 feet from the source)								
(c) Low Biodegradation	7.9	604	6.9	30	1580	9210	1.71e5	1.76e6
(d) High Biodegradation	7.9	740	0.079	30	1580	7610	3330	1.55e6

Table 7 Model results for four scenarios showing a comparison of best and worst cases for the four outputs (first arrival time, maximum concentration, duration and risk).

Table 8 shows a comparison of the parameters across the scenarios. This comparison was made to determine if the extreme cases were generated by the same sets of parameters, despite changes in the average values of the parameter. These results imply that it is possible to determine a generic set of worst case parameters for three of the outputs (first arrival time, maximum concentration and duration above the threshold). In some cases the results are insensitive to a given parameter and either parameter could generate the worst case. For example, the first arrival is independent of release duration in these cases, because the release duration was much greater than the arrival times. Generally the results were consistent for the first arrival, maximum concentration and duration. Definition of the worst case for risk, however, was less clear as the parameter sets were not the same for each simulation. The porosity, fraction organic carbon, dispersivity and half life were different for the scenarios and suggested that a generic set of parameters did not exist for risk.

Note that each of these generic results rests upon the assumption that the model is a valid representation of contaminant transport at a site. At fractured rock or karst sites, sites where pumping wells dominate flow, or for transport in multi-layer aquifers, a more powerful model is required. These models have differing sensitivities to parameters and even different required parameters. Thus a complete assessment depends also on uncertainty associated with the degree of correspondence between the simulation code and the conceptual model of the site.

Uncertainty in model inputs results from spatial variablilty and incomplete or imperfect sampling methods. Running all combinations of input parameters gives bounds on the plausible

outputs of the model.   For each individual parameter set selected for analysis, the worst case parameters varied with the output of interest (i.e., first arrival time, maximum concentration, duration, and risk). Given the chosen output, however, the worst case parameter sets were the same for each combination of hydraulic conductivity and biodegradation rate for the first three outputs.   In contrast, the results for the risk calculation, perhaps because it depends strongly upon both the concentrations and the duration of the breakthrough curve, had no consistent set of worst case parameters. For risk the uncertainty analysis must be performed individually for each parameter set, while for the others this analysis showed a that a generic set of worst case parameters existed. Because this problem is one of transient transport concentrations differ over the duration of exposure. For a steady state model, however, risk could be calculated directly from concentration and there does exist a generic worst case parameter set for this problem.

Scenario	Hydraulic Conductivity	Porosity	Gradient	Fraction organic carbon	Koc	Dispersivity	Half Life	Source conc	SourceDuration
Earliest First Arrival									
Low Conductivity, Low Biodegradation	H	L	H	L	L	H	E	H	E
Low Conductivity, High Biodegradation	H	L	H	L	L	H	E	H	E
High Conductivity, Low Biodegradation	H	L	H	L	L	H	E	H	E
High Conductivity, High Biodegradation	H	L	H	L	L	H	E	H	E
Highest Maximum Concentration									
Low Conductivity, Low Biodegradation	H	L	H	E	E	H	H	H	E
Low Conductivity, High Biodegradation	H	L	H	E	E	H	H	H	E
High Conductivity, Low Biodegradation	H	L	H	E	E	E	H	H	E
High Conductivity, High Biodegradation	H	L	H	E	E	H	H	H	E
Longest Duration									
Low Conductivity, Low Biodegradation	L	H	L	H	H	H	H	H	H
Low Conductivity, High Biodegradation	L	H	L	H	H	H	H	H	H
High Conductivity, Low Biodegradation	L	H	L	H	H	H	E	H	H
High Conductivity, High Biodegradation	L	H	L	H	H	H	H	H	H
Highest Risk									
Low Conductivity, Low Biodegradation	L	H	H	H	H	L	L	H	H
Low Conductivity, High Biodegradation	L	H	H	H	H	L	L	H	H
High Conductivity, Low Biodegradation	L	E	L	E	E	H	E	H	H
High Conductivity, High Biodegradation	L	L	L	H	L	H	H	H	H
H = high value, L = low value, E = either value									

Table 8   Comparison of data sets giving the worst cases for each of four model outputs.

Concentration Uncertainty Model Input and Output

The inputs required for the concentration uncertainty model define the fixed and variable parameters. It is presumed that the distance to the receptor, the chemical of concern and the minimum concentration are all fixed (Figure 23). The remaining parameters of the model can be variable (Figure 24). These include the formal parameters of the transport equation, and parameters that describe the forcing function (source concentration and duration). Each of these parameters can be individually fixed by entering the same value as both "low" and "high" on the input screen. Each parameter that is fixed to a single value reduces the number of model runs by a power of two.

Figure 23 Fixed parameters required for the Concentration Uncertainty model.

Figure 24 Potentially variable parameters required for the Concentration Uncertainty model.

Model Outputs

The major outputs of the model are displayed on three output screens. The first of the output screens shows the values of all the key outputs of the model: first arrival time, maximum concentration, duration above threshold concentration and the risk factor (Figure 25). These are each show for the best and worst case. In addition to displaying the value of the parameter of interest, say the first arrival time, each line of output also shows the associated values of all other outputs.

If it could be determined that a generic set of best and worst case parameter existed, then it would not be necessary to run an uncertainty analysis every time the model was run. Figure 26 indicates which parameter (low or high value) resulted in each model outcome. From these it has been shown that generic worst cases exist for some of the outputs. (See the example problem outputs and discussion.)

Thirdly, the output breakthrough curves are plotted against the breakthrough curve for the average of all input values. These plots show the wide range of possible model outcomes (Figure 27). The families of curves can be moved closer together by fixing values of variable input parameters. Exploring which parameters could benefit from improved estimates can help focus site assessment activities.

		First arrival	Max. Conc.	Duration	Risk Factor
Background	Cases Tested	485			
Select a Model					
Fixed Inputs	Earliest First Arrival	0.2549	29.98	1602.0	152800.0
Variable Inputs	Latest First Arrival	139.5	9.801	3181.0	63920.0
Outputs	Lowest Max. Conc.	9.861	9.745	4132.0	127900.0
Parameter Results	Highest Max. Conc.	0.5240	29.98	3210.0	314100.0
Graphical Output	Shortest Duration	4.170	9.989	1505.0	1780.0
Comparison with Median	Longest Duration	8.526	29.60	6281.0	881400.0
About	Lowest Risk	4.170	9.989	1505.0	1780.0
	Highest Risk	1.705	29.92	3678.0	897900.0
Run	Resume		Pause		Stop

Figure 25 Output from the Concentration Uncertainty model showing the extreme values for each model output: first arrival, maximum concentration, duration above threshold and risk factor.

	Low Value	High Value
Earliest First Arrival	Por Foc Koc Dur	K Grad H.L. Disp C0
Latest First Arrival	K Grad H.L. Disp C0	Por Foc Koc Dur
Lowest Max. Conc.	K Grad H.L. C0 Dur	Por Foc Koc Disp
Highest Max. Conc.	Por	K Grad Foc Koc H.L. Disp C0 Dur
Shortest Duration	Por Foc Koc H.L. Disp C0 Dur	K Grad
Longest Duration	K Grad	Por Foc Koc H.L. Disp C0 Dur
Lowest Risk	Por Foc Koc H.L. Disp C0 Dur	K Grad
Highest Risk	K	Por Grad Foc Koc H.L. Disp C0 Dur

Figure 26 Generic values (low or high) of parameter sets that generate extreme values of each output of the model: first arrival time, maximum concentration, duration and risk factor.
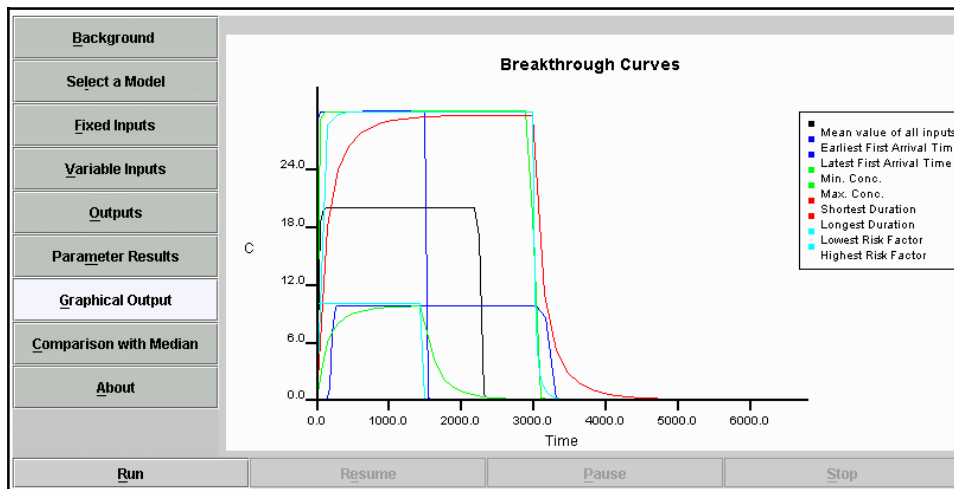
Figure 27 Graphical presentation of Concentration Uncertainty model output showing a comparison of the breakthrough curves for the extremes of each model output: first arrival time, maximum concentration, duration, and risk factor with the breakthrough curve for the average value of all inputs.

36

4. Model Input Parameters

The simulation models described above require input parameters that can be estimated in various ways. The transport equation given above (equation 24) requires six input parameters:

- the retardation factor, R,
- the seepage velocity, v_x,
- the dispersion coefficients in x, y and z (D_x, D_y, and D_z), and
- the loss rate constant, λ.

The next sections describe available methods for estimating or manipulating these parameters.

Retardation Factor Calculator[9]

The retardation factor expresses the amount of sorption of an organic chemical on aquifer solids. This concept is found in the majority of common transport models and is itself a model, as it represents a simplified conceptualization of sorption. The retardation factor is calculated from

$$R \quad = \quad 1 \ + \ \frac{\rho_b}{\theta} k_d \tag{7}$$

where R is the dimensionless retardation factor, ρ_b is the bulk density of the aquifer material [M/L^3], θ is the porosity [L^3/L^3] and k_d is the soil-water distribution coefficient [L^3/M]. The bulk density is related to the porosity

$$
\begin{aligned}
\rho_b \quad &= \quad \rho_s (1 - \theta) \\
&= \quad 2.65 \frac{g}{ml} (1 - \theta)
\end{aligned}
\tag{8}
$$

where ρ_s is the solids density [M/L^3] which is commonly taken as 2.65 g/ml: the density of quartz. The use of bulk density reflects the fact that aquifer materials are composed of both solids and void space.

The soil-water distribution coefficient, k_d, is commonly estimated as the product of the fraction of organic carbon in soil [dimensionless] and the organic carbon partition coefficient, K_{oc} [L^3/M]. K_{oc} has been tabulated or estimated and values are available for most contaminants of concern.

---

[9]http://www.epa.gov/athens/learn2model/part-two/onsite/retard.htm

Example

Retardation factors for benzene and MTBE are given in Tables 10 and 10. These values are presented for varying conditions: low organic carbon (f_{oc} = 0.0001), medium organic carbon (f_{oc} = 0.001); and porosity of 0.25 versus 0.15. The range of K_{oc}'s is taken from data currently in the calculator and is illustrative of the range of possible variation. For benzene (Table 9) the Koc range is taken as 38 L/Kg to 100 L/Kg. This results in insignificant differences in the retardation factor for low values of organic carbon. At the medium organic carbon level (0.0001), the differences in R become more pronounced as the porosity decreases. For MTBE the range of variation in K_{oc} is low, so the differences in R are attributable to the porosity and organic carbon content. Table 10 shows that the highest R for MTBE (1.2) occurs with the lowest porosity and highest organic carbon content (0.15 and 0.001, respectively).

Porosity	Fraction Organic Carbon	Organic Carbon Partition Coefficient (L/Kg)	Retardation Factor
Benzene			
0.15	0.0001	38	1.1
		65	1.1
		83	1.1
		100	1.2
	0.001	38	1.6
		65	2.0
		83	2.2
		100	2.5
0.25	0.0001	38	1.0
		65	1.1
		83	1.1
		100	1.1
	0.001	38	1.3
		65	1.5
		83	1.7
		100	1.8

Table 9 Retardation factors for benzene under varying conditions.

Porosity	Fraction Organic Carbon	Organic Carbon Partition Coefficient (L/Kg)	Retardation Factor
MTBE			
0.15	0.0001	11	1.0
		14	1.0
0.15	0.001	11	1.2
		14	1.2
0.25	0.0001	11	1.0
		14	1.0
0.25	0.001	11	1.1
		14	1.1

Table 10 Retardation factors for MTBE under varying conditions.

Ground Water Velocity

Seepage Velocity Calculator[10]

On average, the velocity of a contaminant is governed by the seepage velocity[11], v_s, which is the Darcy Flux divided by the porosity.

$$v_s = -\frac{K}{\theta} i \qquad (9)$$

where K is the hydraulic conductivity [L/T], θ is the porosity [L^3/L^3], and i is the hydraulic gradient [L/L]. Equation 9 gives the magnitude of the gradient as a scalar quantity. Velocity is, obviously, directional and the gradient establishes the direction[12].

---

[10]http://www.epa.gov/athens/learn2model/part-two/onsite/seepage.htm

[11]Seepage velocity is also know by the term average linear velocity and others.

[12]In non-isotropic media, the direction is also determined by the hydraulic conductivity tensor.

Hydraulic Gradient Calculator[13]

The magnitude and direction of the hydraulic gradient can be estimated by fitting a plane through the ground water surface. The equation of the plane is

$$a\,x \; + \; b\,y \; + \; c \;\; = \;\; h \tag{10}$$

where x and y are the coordinates of a well, h is the hydraulic head, and a,b, and c are constants. The constants can be evaluated by fitting the plane to at least three wells. When more than three points are used, the coefficients are calculated by least-squares fitting of the data to the plane. The magnitude of the gradient is calculated from the square root of $a^2 + b^2$, the direction from North is determined from the arctangent of a/b or b/a, depending on the quadrant.

Example

Water level data from four wells on a service station are shown in Table 11. These were used to calculate the magnitude and direction of the gradient for six dates from 1991 to 1998. Note that the locations (x and y) and elevations of the top of casing for each well are necessary for calculating the gradient. In this case the x and y coordinates were scaled from a map and the elevations were determined by a survey. Figure 28 shows the resulting directions and magnitudes. Clearly, these results are not consistent over time. This result may be due to the very small scale covered by the data, and the high proportion of pavement at the site. Note that when the direction is indicated to be about 90 degrees (East), the magnitude of the gradient is small. These times correspond to nearly identical water levels in the wells (Table 11, data from 3/20/1994 and 4/22/1998), and for this reasone these flat gradients may not be accurate. Also, this site is located just to the east of the Mississippi River, and the expected direction of flow would be to the West. To determine the gradient more definitively, wells are needed beyond the boundaries of the service station property and the regional ground water flow direction needs to be considered.

---

[13]http://www.epa.gov/athens/learn2model/part-two/onsite/gradient4plus-ns.htm
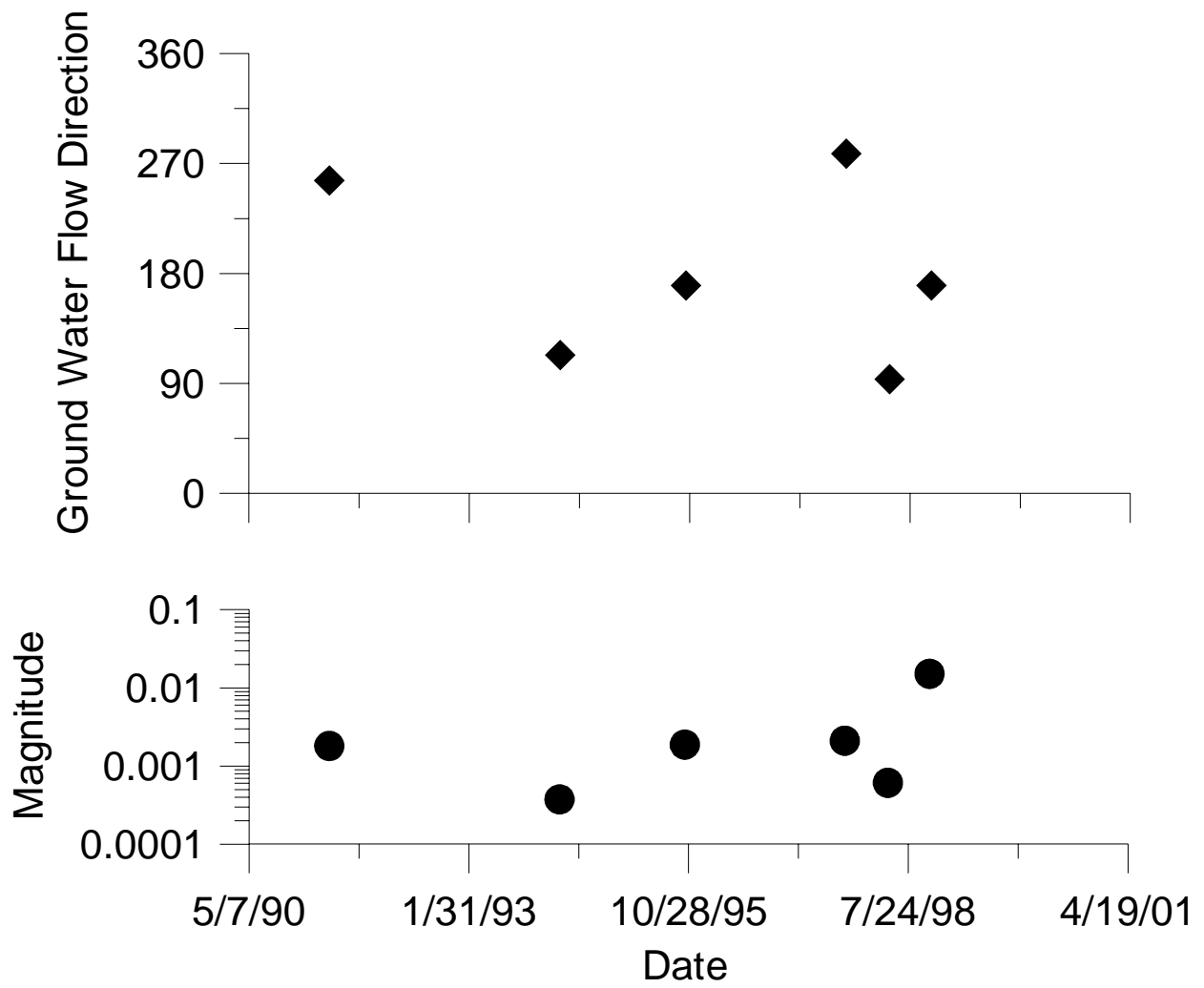
Figure 28 Magnitude and direction of gradient for example site.

Date	Well	Coordinates (ft)		Elevation TOC[1] (ft)	Depth to Water (ft)	Elevation Water (ft)
		East	North			
5/7/1991	MW-1	133	99	499.11	48.08	451.03
	MW-2	123	38	499.19	48.21	450.98
	MW-3	100	101	498.83	47.87	450.96
	MW-4	62	89	498.63	47.73	450.9
3/20/1994	MW-1	133	99	499.11	49.27	449.84
	MW-2	123	38	499.19	49.37	449.82
	MW-3	100	101	498.83	49.01	449.82
	MW-4	62	89	498.63	48.77	449.86
10/11/1995	MW-1	133	99	499.11	49.31	449.8
	MW-2	123	38	499.19	49.52	449.67
	MW-3	100	101	498.83	49.06	449.77
	MW-4	62	89	498.63	48.83	449.8
10/8/1997	MW-1	133	99	499.11	48.79	450.32
	MW-2	123	38	499.19	48.7	450.49
	MW-3	100	101	498.83	48.2	450.63
	MW-4	62	89	498.63	48.42	450.21
4/22/1998	MW-1	133	99	499.11	47.99	451.12
	MW-2	123	38	499.19	48.08	451.11
	MW-3	100	101	498.83	47.72	451.11
	MW-4	62	89	498.63	47.47	451.16
10/29/1998	MW-1	133	99	499.11	48.87	450.24
	MW-2	123	38	499.19	49.89	449.3
	MW-3	100	101	498.83	48.6	450.23
	MW-4	62	89	498.63	48.37	450.26
						[1] TOC stands for top of casing.

Table 11 Data for gradient calculation example.

Longitudinal Dispersion Coefficient Calculator[14]

As discussed previously, the dispersion coefficient appearing in the transport equation (24) represents differential advection, is not measured at LUST sites, and is best treated as a fitting parameter. Data have been collected on dispersion coefficients, however, that provide insight into the dispersion parameter. Gelhar et al. (1992) published a review of dispersivities (D/v_s) which is replotted in Figure 29. Because the data ***do not*** plot on a horizontal line, These data show scale-dependence of dispersivity. This fact implies that no single value represents a contaminant plume. From this follows the conclusion that dispersivity should be treated as a fitting parameter. Various methods have been devised to estimate dispersivity for a specific site from the Gelhar et al. (1992) tabulation. Two of these are shown in Figure 30 (see Xu and Eckstein, 1995). Without comparing values generated from these formulas to the underlying data, a false sense of certainty may be perceived. At a given scale the tabulated dispersivities can range over three orders of magnitude. The formulas, of course, give specific values.

In order to give a sense of the formula values and the range of variability, the dispersivity calculator produces estimates from two formulas, and an evident range from the tabulation. Table 12 gives values for various plume lengths (an indicator of the problem scale) and the estimated range of values in the tabulation. From these results one can conclude that the range of literature variability of this parameter is very high and that in the absence of fitting to observed concentrations there is no way to prove that a chosen value is appropriate.[15]

---

[14]http://www.epa.gov/athens/learn2model/part-two/onsite/longdisp.htm

[15]The converse is also true: it is not possible to prove values are inappropriate in the absence of fitting.
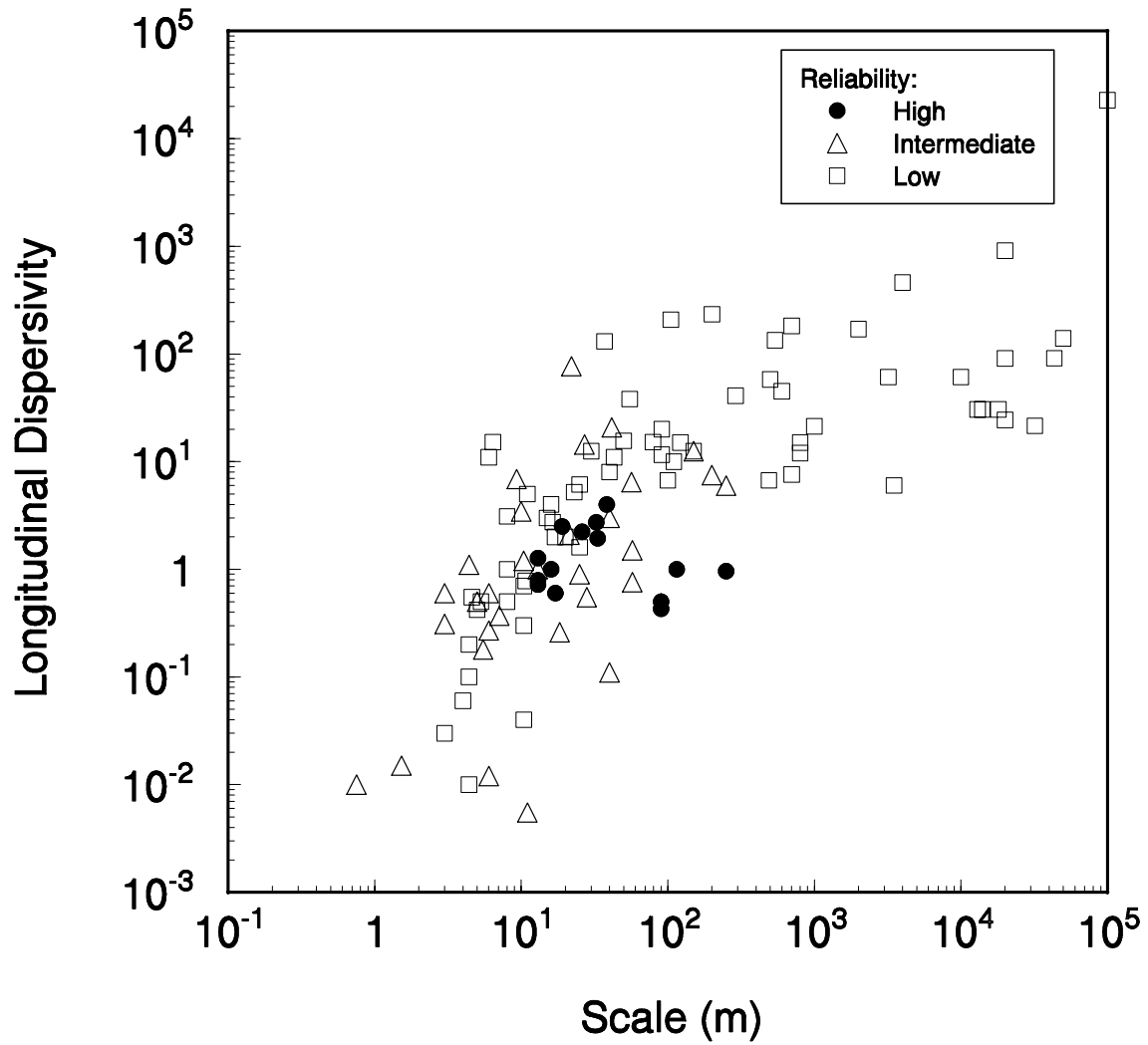
Figure 29 Data tabulation from Gelhar et al. (1992) showing published longitudinal dispersivity as a function of scale.

Figure 30 Gelhar et al. (1992) dispersivity tabulation with scale-related estimates.

Plume Length (ft)	Approximate Lower Bound (ft)	Xu and Eckstein Formula Result (ft)	Approximate Upper Bound (ft)
100	0.084	7.06	670
500	0.95	17.9	2800
1000	1.7	24.5	5200
2500	3.9	35.1	12000
5000	6.3	44.6	19000

Table 12 Relationships between plume length, data scatter on the Gelhar (1992) tabulation and the Xu and Eckstein (1995) formula.

Half-Lives to Rate Constant Conversion Calculator[16]

Laboratory microcosm data are often reported in terms of representative first-order rate constants, λ. The rate constant is also required as input for most models that use this concept. The rate constant can be represented as a half-life, through a simple conversion.

The equation for first-order decay is the starting point for determining the conversion factor:

$$\frac{dC}{dt} = -\lambda C \tag{11}$$

where C is the concentration, t is time, and λ is the first-order rate constant. The solution to equation 11 is given by

$$C(t) = C_o \exp[-\lambda(t - t_o)] \tag{12}$$

where C(t) is the concentration at time t, C_o is the intial concentration, and t_o is the initial time. The half life, $t_{1/2}$ is obtained by setting the concentration equal to one-half its initial value in equation 12. After rearranging and taking the natural log (ln) of both sides, the half life becomes

---

[16]http://www.epa.gov/athens/learn2model/part-two/onsite/halflife.htm

$$\ln(\frac{1}{2}) \quad = \quad - \lambda \, t_{1/2} \tag{13}$$

When the log of ½ is evaluated, the conversion is seen to be

$$t_{1/2} \quad = \quad \frac{0.6931}{\lambda} \tag{14}$$

Additional Parameter Values

There are a number of other parameters that are used in models of various types. These will be discussed in the following sections: the effective solubility from a mixture, henry's constants and diffusion coefficients.

Effective Solubility from Mixture Calculator[17]

The concentration of a chemical in equilibrium with a water-immiscible mixture differs from the solubility of that chemical in equilibrium with water alone. The solubility resulting from the mixture is called the effective solubility and depends on the pure component solubility (water alone) and the amount of chemical in the mixture (mixture properties).   Raoult's Law is used to characterize the partitioning and is stated as:

$$S_{eff} \quad = \quad x_i S_i \tag{15}$$

where S_{eff} is the effective solubility of a chemical in a mixture [M/L^3], x_i is the mole fraction of the chemical in the mixture [M/M] and S_i is the solubility of the chemical in water [M/L^3]. In this formulation the activity of the chemical in the mixture has been assumed equal to one, following the work of Cline et al. (1991) for gasolines.   Effective solubilities, thus depend on the composition of the mixture (the mole fraction) and the solubility of the chemical of interest. These solubilities may in turn vary with temperature as described in the next section.

Shallow Ground Water Temperature in the United States

Average shallow ground water temperatures range from 5 °C in the North to 25 °C in southern Florida (Figure 31). These values give an indication of the range of temperature dependence that might be encountered on a nationwide scale.

---

[17]http://www.epa.gov/athens/learn2model/part-two/onsite/es.htm
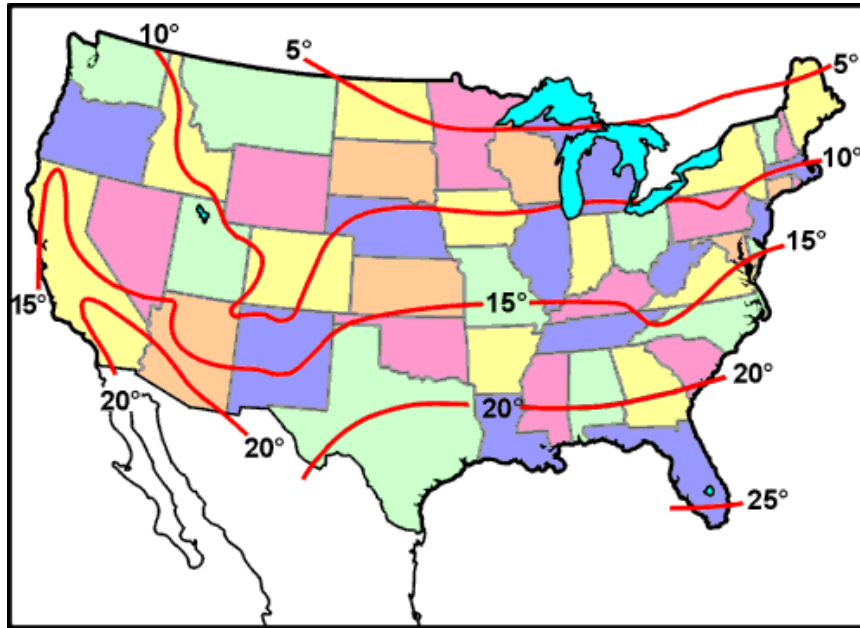
Figure 31 Shallow ground water temperatures throughout the United States.

Temperature Dependence of MTBE, Benzene and Toluene Solubility

Temperature dependence in effective solubility is introduced through data on methyl tert-butyl ether (MBTE) and benzene solubilities over the range of 0 ºC to 40 ºC. These data are drawn from Peters et al. (2002) and Montegomery (1996). Some comments are needed on these data:

- The temperature-dependent effective solubility calculator uses the assumptions concerning Raoult's law described above:
  - Mixture properties are approximated by the average properties of the fuel
  - Unitary activity coefficients
- Inconsistent solubility data reported in the scientific literature is the *rule* rather than the exception.
- As new or improved data become available the calculator will be updated.
- The MTBE solubilities from Peters et al. (2002), do not match the commonly used value of about 50 g/L at 25 ºC. The Peters et al., data do, however, roughly match two data points reported by Fischer et al. (2004) , and the value reported given in the Handbook of Chemistry and Physics (Lide, 2000)
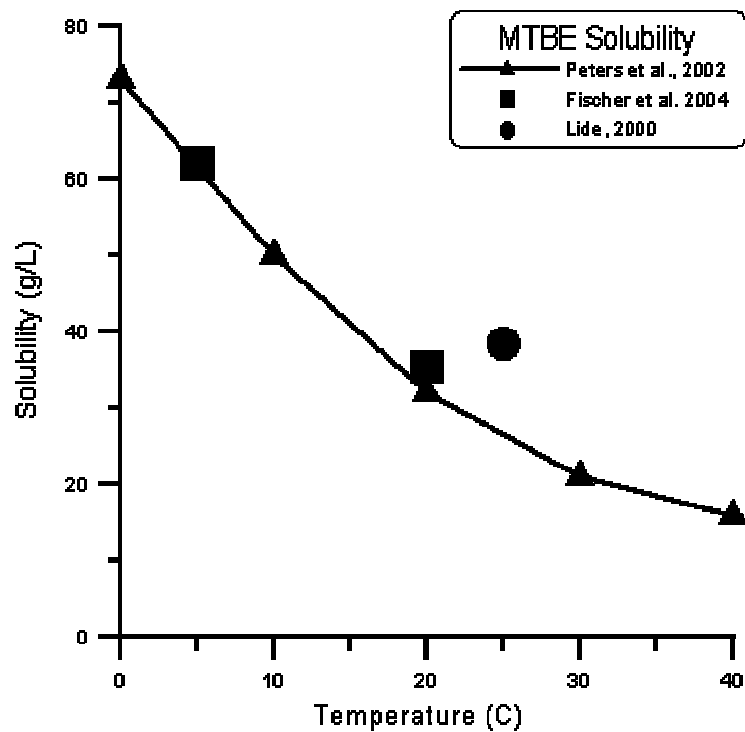
Figure 32 Graph of MTBE solubility versus temperature
showing decline in solubility with increasing temperature.

MTBE

The calculator uses the data points from Peters et al. (triangles on Figure 32) and linear interpolation to estimate the MTBE solubility. Other data that would more fully establish the temperature-dependent solubility of MTBE do not exist.

Benzene

The benzene data are taken from a larger list of contradictory data presented by Montegomery, but these (Stephens and Stephens, 1963) data were selected on the basis of their agreement with the reported solubility of benzene at 25 °C (Figure 33).
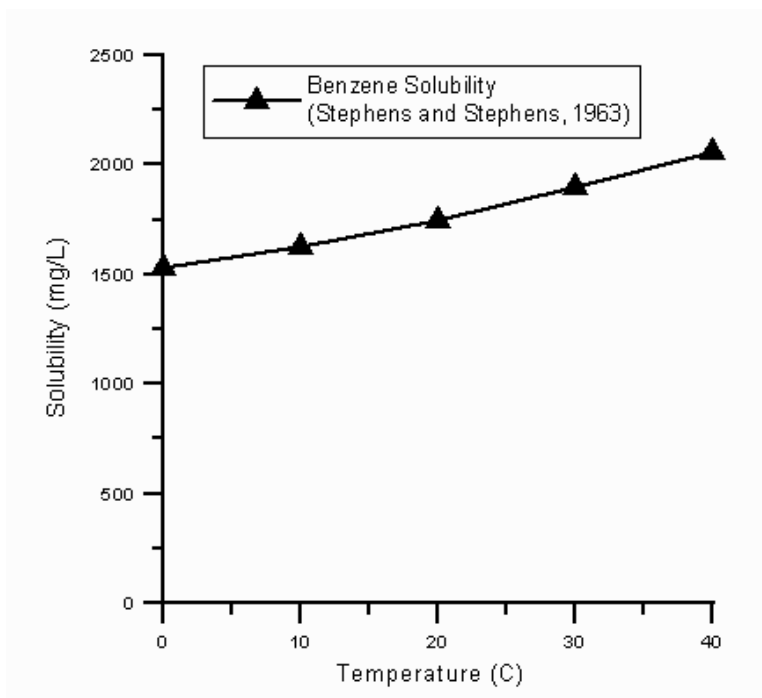
Figure 33 Graph of benzene solubility versus temperature
showing modest increase in solubility with increasing
temperature.

The International Union of Pure and Applied Chemistry (IUPAC) has evaluated benzene
data from many sources and prepared a set of recommended values or best values for temperatures
from 0 ºC to 80 ºC. Over the range of 0 ºC to 25 ºC the IUPAC data and its ranges encompasses
the Stephens and Stephens (1963) data (Figure 33).   IUPAC, however, shows that the solubility
of Benzene remains roughly constant over this range. The data point for 0 ºC is a "best" value
rather a "recommeded" value, because of more uncertainty at 0 ºC. Table 13 shows the values and
ranges plotted in Figure 34.

50

Temperature	Lower 95% Confidence Limit	IUPAC Best or Recommended Value	Upper 95% Confidence Limit
ᵒC	mg/L	mg/L	mg/L
0	1372	1693	2013
5	1753	1803	1853
10	1743	1783	1823
15	1723	1763	1803
20	1733	1763	1793
25	1753	1773	1793

Table 13 IUPAC benzene solubility data.
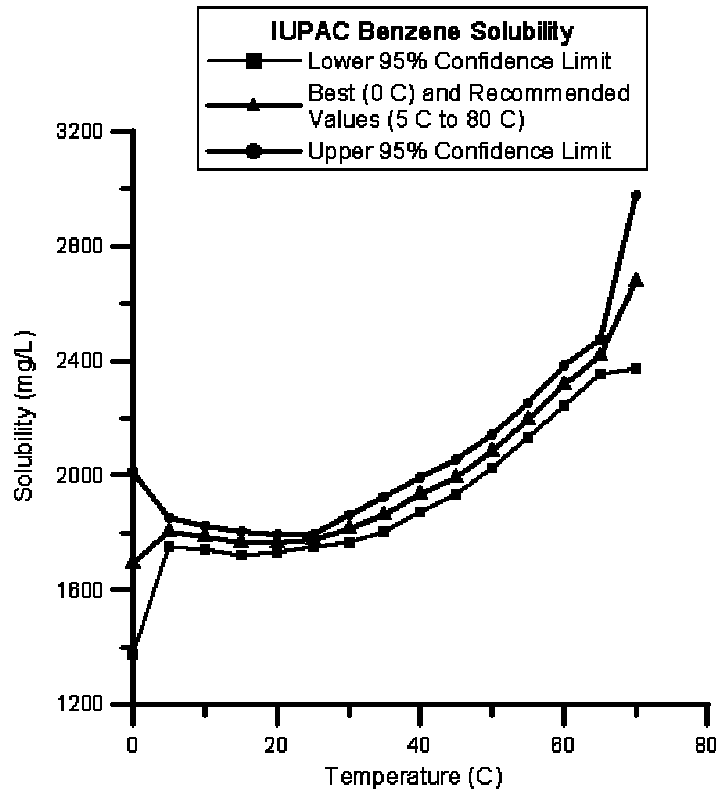
Figure 34 IUPAC data on benzene solubility showing the lower 95% confidence limit, recommended value, and upper 95% confidence limit.

51

Other sources of chemical data can be found on the ERD chemical properties page at
http://www.epa.gov/athens/research/regsupport/properties.html

Toluene

     The IUPAC prepared data on toluene (Figure 52) and prepared a set of best values for temperatures from 0 ºC to 60 ºC. The following table shows the ranges of values for toluene and lower and upper ranges. These data were judged to be of generally lower quality and only "best" values rather than "recommended" values were given.
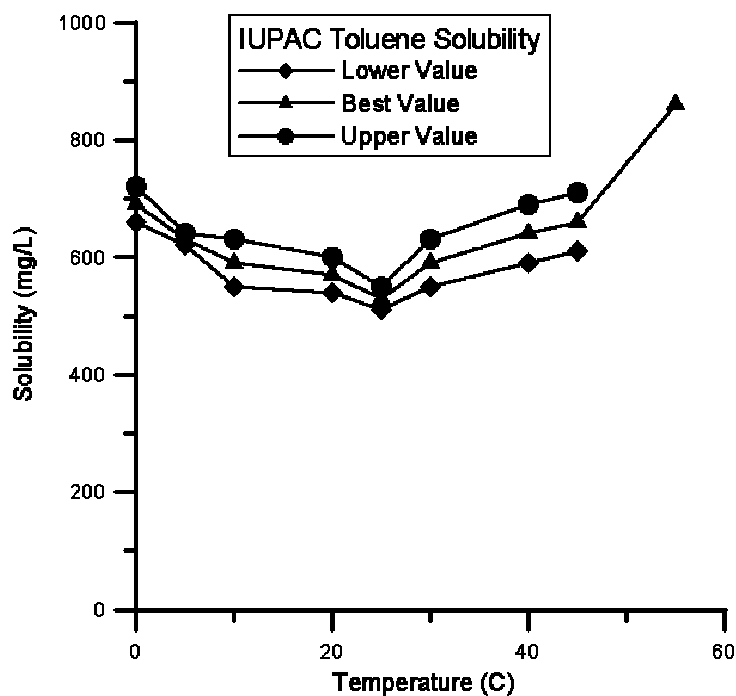
Figure 35 IUPAC data on toluene solubility showing the lower value, best value, and upper value.

Temperature	Lower 95% Confidence Limit	IUPAC Best or Value	Upper 95% Confidence Limit
ºC	mg/L	mg/L	mg/L
0	660	690	720
5	620	630	640
10	550	590	630
20	540	570	600
25	510	530	550

Table 14 IUPAC toluene solubility data.

Example Values

Table 15 shows effective solubilities for benzene and MTBE for temperatures of 5 ºC, 15 ºC and 25 ºC. Since the effective solubility depends on the mass fraction of the chemical in the fuel, the table includes values for example fuels. These fuels contain varying amounts of benzene and MTBE and the choices used in the table reflect a range of possibilities. The effective solubilities also depend strongly on the presumed temperature-dependent solubilities for each chemical. In every case the effective solubilities are far less than the solubilities. For a given temperature, though, the effective solubility increases with mass fraction in the fuel. The variation of effective solubility with temperature is show in Table 16. It is evident that most, if not all the variation is due to the variation of solubility itself.

Chemical	Solubility mg/L	Effective Solubilities (mg/l) for indicated % mass fraction		
benzene mass fractions:		0.398 [1]	0.453 [2]	0.845 [3]
5 ºC	1480	7.9	9.0	16.8
15 ºC	1570	8.4	9.6	17.8
25 ºC	1680	8.9	10.	19.
MTBE mass fractions:		1.52 [4]	10.4 [5]	12.2 [6]
5 ºC	84500	1530	10300	12100
15 ºC	59000	1070	7180	8420
25 ºC	37500	678	4560	5350
[1] 93 Octane gasoline, MTBE [2] 93 Octane gasoline, non-MTBE [3] 87 Octane gasoline, Low MTBE [4] 93 Octane gasoline, Low MTBE [5] 87 Octane gasoline, MTBE [6] 93 Octane gasoline, Low MTBE				

Table 15 Example effective solubilities for benzene and MTBE at temperatures of 5ºC, 15ºC and 25 ºC.

Chemical	% Range in Solubility	% Variation in Effective Solubilities for indicated % mass fraction		
benzene mass fractions:		0.398 [1]	0.453 [2]	0.845 [3]
% variation 5 ºC to 25 ºC	11.9%	11.2%	10%	11.6%
MTBE mass fractions:		1.52[4]	10.4[5]	12.2[6]
% variation 5 ºC to 25 ºC	55.6%	55.7%	55.7%	55.8%
[1]93 Octane gasoline, MTBE [2]93 Octane gasoline, non-MTBE [3]87 Octane gasoline, Low MTBE [4]93 Octane gasoline, Low MTBE [5]87 Octane gasoline, MTBE [6]93 Octane gasoline, Low MTBE				

Table 16 Range of variation of effective solubilities for benzene and MTBE from 5ºC to 25 ºC.

Temperature-Dependent Henry's Law Coefficient Calculator[18]

Henry's constants represent equilibrium partitioning between a chemical in water and the air. If the concentrations in water, C_w, and air, C_a are given in units of mg/L, then the nominally dimensionless Henry's law coefficient, H_{cc} is given by

$$C_a \quad = \quad H_{cc} C_w \tag{16}$$

The concentrations may be expressed in differing unit sets, however, and the corresponding Henry's Law coefficients differ from the dimensionless values. Staudinger and Roberts (1996, page 292) give the relationships between the four Henry's constant unit sets listed in Table 17. The relationships between the values of the four unit sets was given by Staudinger and Roberts (1996) by the formula:

$$H_{cc} \quad = \quad H_{yx}\left(\frac{MW_L}{\rho_L}\right)\left(\frac{\rho_G}{MW_G}\right) \quad = \quad H_{px}\left(\frac{1}{RT}\right)\left(\frac{MW_L}{\rho_L}\right) \quad = \quad H_{pc}\left(\frac{1}{RT}\right) \tag{17}$$

where MW_G and MW_L are the molecular weights [M] of the gas (G) and liquid (L) respectively, ρ_G and ρ_L are the densities [M/L^3] of the gas and liquid, T is the temperature in K, and R is the universal gas constant. Table 18 gives values of the constants required for performing the unit conversions. Equation 18 gives the conversion factors for ambient conditions (pressure of 1 atm).

$$ H_{cc} = H_{yx} \left(\frac{0.2194}{T} \right) = H_{px} \left(\frac{0.2194}{T} \right) = H_{pc} \left(\frac{12,186}{T} \right) \qquad (18) $$

Concentration Representations: Air/Water	Symbol	units
Concentration/Concentration	Hcc	(dimensionless--volumetric basis)
Mole Fraction Y / Mole Fraction X	Hyx	(dimensionless)
Partial Pressure / Mole Fraction X	Hpx	(atmospheres)
Partial Pressure / Solubility	Hpc	(atm m^3/mol)

Table 17   Unit sets for Henry's Constants.

Quantity	Symbol	Value
molecular weight of water	MW_L	0.018 kg/mole
density of water	ρ_L	1000 kg/m^3
molecular weight of air	MW_G	0.029 kg/mole
universal gas constant	R	82.06 x 10^{-6} atm m^3/mol K

Table 18 Constants needed for Henry's law unit conversions.

Example Values

Values of Henry's contants are given in Table 19 for benzene, MTBE, perchloroethene (PCE) and trichloroethene (TCE). Values are given for both the OSWER and Washington (1996) methods. The two sets of results show generally close agreement. As illustrated by MTBE, data may not be available for each chemical in each method. Over the range of temperatures of 5 $^\circ$C to 25 $^\circ$C, the Henry's constants vary by about 50 % to 70%.

56

Chemical	Estimated Henry's Law Coefficient			
	OSWER Method (dimensionless)	% variation 5 $^{\circ}$C to 25 $^{\circ}$C	Washington (1996) Method (dimensionless)	% variation 5 $^{\circ}$C to 25 $^{\circ}$C
Benzene				
5	0.0887	60.9%	0.106	50.5%
15	0.145		0.152	
25	0.227		0.214	
MTBE				
5	-- [a]	--[a]	0.0101	61.5%
15	--[a]		0.0165	
25	--[a]		0.0262	
Perchloroethene (PCE)				
5	0.245	66.5%	0.232	67.4%
15	0.441		0.415	
25	0.752		0.711	
Trichloroethene (TCE)				
5	0.156	62.9%	0.137	63.2%
15	0.263		0.230	
25	0.421		0.372	
[a]Data not available for calculation.				

Table 19 Estimated Henry's law coefficients for benzene, MTBE, perchloroethene and trichloroethene at temperatures of 5 $^{\circ}$C, 15 $^{\circ}$C, and 25 $^{\circ}$C.

Diffusion Coefficient Calculator[19]

The estimates of diffusion coefficients are developed from methods presented by Tucker and Nelken (1990). The calculator uses three methods to make estimates of diffusion coefficients in air: Fuller, Schettler and Giddings (FSG), the LaBas modification of FSG (FSG-LaBas) and Wilke and Lee (WL), and one method for the diffusion coefficient in water: Hayduk and Laudie (HL). Each of these are described briefly in Appendix 6, with complete details given in the reference (Tucker and Nelken, 1990).

Example Input and Output Values

Table 20 shows the values of inputs to define four chemicals: benzene, MTBE, perchloroethene (PCE) and trichloroethene (TCE).   The calculator requires the input of the numbers of atoms in the molecule, the number of aromatic rings, special conditions for oxygen and nitrogen, pressure, temperature and boiling point. The calculation is applicable to chemicals containing only the atoms displayed (hydrogen, carbon, nitrogen, oxygen, sulfur, fluorine, chlorine, bromine and iodine) and, if rings are present, they are only aromatic (6-carbon) rings. Adjustments are made internally for oxygen in the form of esters or ethers, in acids or joined to sulphur or nitrogen. Adjustment are also made for amine nitrogen and double-bonded nitrogen. The boiling point of the chemical is needed for the WL method.   The values appearing in Table 58 were obtained from Aldrich Chemical Company (2003).

Table 21 shows estimated air and water phase diffusivities for the four chemicals. The values were estimated by each of the methods described above (FSG, FSG-LaBas, WL for air, and HL for water). Because the estimation methods depend upon the volume occupied by each molecule either in air or water, the values vary little and tend to be on the order of 10^{-2} cm^2/s for the air phase and 10^{-6} cm^2/s for water. The values given in Table 21, are generally of this magnitude and also show little variability with temperature.

Chemical	Number of atoms				Aromatic Rings	Oxygen conditions	Nitrogen conditions	Boiling point (^{o}C)
	hydrogen	carbon	oxygen	chlorine				
benzene	6	6	0	0	1	n/a	n/a	80
MTBE	12	5	1	0	0	higher ethers	n/a	55.5
PCE	0	2	0	4	0	n/a	n/a	121
TCE	1	2	0	3	0	n/a	n/a	86.7

Table 20   Diffusion coefficient calculation input parameters for benzene, MTBE, perchloroethene, and trichlorethene.

Chemical	Diffusion Coefficients in Air (cm^2/s)			Diffusion Coefficient in Water (cm^2/s)
	FSG	FSG-LaBas	WL	HL
Benzene				
5 ℃	0.0792	0.0817	0.0859	5.6 e-6
15 ℃	0.0842	0.0869	0.0919	7.8 e-6
25 ℃	0.0894	0.0923	0.0980	1.0 e-5
MTBE				
5 ℃	0.0714	0.0710	0.0751	4.7 e-6
15 ℃	0.0759	0.0755	0.0803	6.5 e-6
25 ℃	0.0806	0.0802	0.0856	8.6 e-6
Perchloroethene (PCE)				
5 ℃	0.0673	0.0671	0.0711	4.7 e-6
15 ℃	0.0716	0.0713	0.0760	6.6 e-6
25 ℃	0.0760	0.0757	0.0811	8.7 e-7
Trichloroethene (TCE)				
5 ℃	0.0738	0.0737	0.0779	5.3 e-6
15 ℃	0.0785	0.0784	0.0832	7.3 e-6
25 ℃	0.0833	0.0832	0.0888	9.7 e-6

Table 21 Estimated air and water diffusivities for benzene, MTBE, perchloroethene and trichloroethene at temperatures of 5 ℃, 15 ℃, and 25 ℃.

5. Conclusions

A series of on-line tools has been created for assisting in assessing contaminated sites. These tools include simple methods for estimating model inputs. The direct model input tools include the retardation factor, hydraulic gradient, seepage velocity, dispersion coefficients, rate constant/half life conversions. Other tools provide methods and data for estimating the effective solubility of contaminants from fuels, temperature-dependent Henry's constants, and air and water phase diffusivities. These parameters are needed for certain models and the effective solubility can be sued to determine the maximum possible concentration resulting from fuel contamination.

Because few sites are evaluated based on field data alone, models or other calculations are used in site assessment. As stated previously, models are chosen for this task because

- they have an evident ability to predict future concentrations,
- they have a scientific basis,
- they have the ability to include the effects of many different factors, and
- they have become accepted as predictive tools.

A number of factors, however, influence and limit the ability of models to predict future contamination. This report focused on uncertainty in parameter values. For the prediction of plume diving, recharge estimates are critical, but may be difficult to obtain. Here the model is used as a tool for the best placement of well screens. Subsequent data collection would confirm the prediction, but, more importantly, would be of higher quality because of the inclusion of this theory in well placement. Parameter uncertainty in contaminant transport showed that a wide variety of breakthrough curves could be generated from a set of inputs. Where the inputs are not completely know, this behavior of the model is a truer representation of the results than a model run using averaged parameters. If, however, through uncertainty analysis it can be shown that generic best and worst cases exist, then bounding results could be generated. For the one-dimensional contaminant transport model studied here, generic worst/best cases can be established for the first arrival time, maximum concentration and duration. The parameter sets that generate these do not generate each of the worst/best cases. When risk is considered to be based on transient concentrations, a generic worst case doesn't exist at all. For these two reasons the existence of universal extreme parameter sets it limited, but may be useful in some cases.

References

Aldrich Chemical Company, 2003 Aldrich Handbook of Fine Chemicals and Laboratory Equipment.

ASTM, 1995, Standard Guide for Risk-Based Corrective Action Applied at Petroleum Release Sites, American Society for Testing and Materials, ASTM Designation E 1739095.

Bear, J., 1972, Dynamics o f Fluids in Porous Media, American Elsevier, New York.

Buscheck, T.E. and C.M. Alacantar, 1995, Regression Techniques and Analytical Solutions to Demonstrate Intrinsic Bioremediation, Intrinsic Bioremediation, Hinchee, R.E., J.T. Wilson, D.C. Downey, eds., Battelle Press, 3(1).

Cline, P.V., J.J. Delfino, P.S.C. Rao, 1991, Partitioning of aromatic constituents into water from gasoline and other complex solvent mixtures, Environmental Science and Technology, 23, 914-920.

Eggleston, J.R. and S. A. Rojstaczer, 2000, Can We Predict Subsurface Mass Transport?, Environmental Science and Technology, 34, 4010-4017.

Fischer, A., M. Muller, J. Klasmeier, 2004, Determination of Henry's law constant for methyl *tert*-butyl ether (MTBE) at groundwater temperatures, Chemosphere, 54, 689-694.

Gelhar, L.W., K.R. Rehfeldt, and C.A. Welty, 1992, A critical review of data on field-scale dispersion in aquifers, Water Resources Research, 28(7), 1955-1974.

Haitjema, H.M., 1995, Analytic Element Modeling of Groundwater Flow, Academic Press, 304pp.

Leij, F.J. and S.A. Bradford, 1994, 3DADE:A computer program for evaluating three-dimensional equilibrium solute transport in porous media, Research Report No. 134, U.S. Salinity Laboratory, Riverside, CA.

Lide, D.R., 2000, CRC Handbook of Chemistry and Physics, 81st ed., CRC Press, page 8-95.

Miller, C.T. and W.G. Gray, 2002, Hydrological Research: Just Getting Started, Ground Water, 40(3), 224-231.

Montegomery, J.H., 1996, Groundwater Chemicals Desk Reference, 2nd ed., CRC Press, Lewis Publishers, Boca Raton, Florida, page 70-71.

Oreskes, N., K. Shrader-Frechette, K. Belitz, 1994, Verification, Validation, and Confirmation of Numerical Models in the Earth Sciences, Science, 263, 641-646.

Peters, U., F. Nierlich, M. Sakuth, and M. Laugier, 2002, Methyl Tert-Butyl Ether, Physical and Chemical Properties, Ullmanns Encyclopedia of Industrial Chemistry, Release 2003, 6th ed., VCH Verlag GmbH & Co. KGaA, Wiley, DOI, 10.1002/14356007.a16_543.

Shaw, D.G., 1989, Solubility Data Series, Hydrocarbon with Water and Seawater, Part I: Hydrocarbons C_5 to C_7, Volume 37, International Union of Pure and Applied Chemistry, Pergamon Press, Oxford.

Strack, O.D.L., 1984, Three-dimensional streamlines in Dupuit-Forchheimer models, Water Resources Research, 20, 812-822.

Staudinger and Roberts, 1996, A Critical Review of Henry's Law Constants for Environmental Applications, in Critical Reviews in Environmental Science and Technology, 26(3):205-297

Stephen, H. and T. Stephen, 1963, Solubilities of Inorganic and Organic Compounds, Vol. 1., Macmillan, New York.

Tucker, W.A., and L.H. Nelken, 1990, Chapter 17: Diffusion Coefficients in Air and Water, Handbook of Chemical Property Estimation Methods. Warren J. Lyman, William F. Reehl and David H. Rosenblatt, eds., first edition, American Chemical Society.

United States Environmental Protection Agency, 1989, Risk Assessment Guidance for Superfund Volume 1, Human Health Evaluation Manual (Part A), Interim Final, Office of Emergency and Remedial Response, Washington, DC, EPA/540/1-89-002.

United States Environmental Protection Agency, 2001, Fact Sheet: Correcting the Henry's Law Coefficient for Temperature, Office of Solid Waste and Emergency Response, http://www.epa.gov/athens/learn2model/part-two/onsite/doc/factsheet.pdf.

van Genuchten, M. T. and W. J. Alves, 1982, Analytical Solutions of the One-Dimensional Convective-Dispersive Solute Transport Equation, United States Department of Agriculture, Agricultural Research Service, Technical Bulletin Number 1661.

Washington, J., 1996, Gas partitioning of dissolved volatile organic compounds in the vadose zone: Principles, temperature effects and literature review, Ground Water, 34(4), 709-718.

Weaver, J.W, J.T. Haas, and J.T. Wilson, 1996, Analysis of the gasoline spill at East Patchogue, New York, Procedings of Non-Aqueous Phase Liquids (NAPLs) in Subsurface Environment: Assessment and Remediation, ed. L. Reddi, American Society of Civil Engineers, Washington, D.C., November 12-14, pp. 707-718.

Weaver, J.W, 1996, Application of the Hydrocarbon Spill Screening Model to Field Sites, Procedings of Non-Aqueous Phase Liquids (NAPLs) in Subsurface Environment: Assessment and

Remediation, ed. L. Reddi, American Society of Civil Engineers, Washington, D.C., November 12-14, pp. 788-799.

Xu, M., and Y. Eckstein, 1995, Use of weighted least-squares method in evaluation of the relationship between dispersivity and scale, Groundwater, 33(6), 905-908.

Appendix 1 Calculator Reference

The calculators described in the text are available on the EPA web site at http://www.epa.gov/athens/onsite. The specific web links for each calculator are given in the following tables: Table 22– models, Table – formulas/model input paramters, and Table – unit conversions.

Method	Name	URL
Average Borehole Concentration	Average BoreHole Concentration	http://www.epa.gov/athens/learn2model/part-two/onsite/abc.htm
Vertical Gradients	Vertical Gradient	http://www.epa.gov/athens/learn2model/part-two/onsite/vgradient.htm
Plume Diving	Plume Diving	http://www.epa.gov/athens/learn2model/part-two/onsite/diving.htm
Uncertainty in Subsurface Transport Calculations	ConcentrationUncertainty	http://www.epa.gov/athens/learn2model/part-two/onsite/uncertainty.htm

Table 22 Web (URLs) for models and associated calculations described in the text.

Method	Name	URL
Retardation Factor	Retardation Factor	http://www.epa.gov/athens/learn2model/part-two/onsite/retard.htm
Ground Water Velocity	Seepage Velocity Hydraulic Gradient	http://www.epa.gov/athens/learn2model/part-two/onsite/seepage.htm http://www.epa.gov/athens/learn2model/part-two/onsite/gradient4plus.htm
Dispersion Coefficient	Dispersion Coefficient	http://www.epa.gov/athens/learn2model/part-two/onsite/longdisp.thm
Half-Lives to Rate Constants	Half Lives and Rate Constants	http://www.epa.gov/athens/learn2model/part-two/onsite/halflife.htm
Effective Solubility	Effective Solubility	http://www.epa.gov/athens/learn2model/part-two/onsite/es.htm http://www.epa.gov/athens/learn2model/part-two/onsite/es-temperature.htm
Henry's Constant	Henry's Constant	http://www.epa.gov/athens/learn2model/part-two/onsite/esthenry.htm
Diffusivity	Diffusivity	http://www.epa.gov/athens/learn2model/part-two/onsite/estdiffusion.htm

Table 23 Web (URLs) for formulas/model inputs described in the text.

Appendix 2 Acronyms and Abbreviations

BTEX	Benzene, toluene, ethylbenzene and xylenes
CoC	Concentration-of-concern
FSG	Fuller, Schettler and Giddings Method for Air Diffusion
IUPAC	International Union of Pure and Applied Chemistry
HL	Hayduk and Laudie Method for Water Diffusion
LUST	Leaking underground storage tank
MCL	Maximum contaminant level
MTBE	Methyl tert-butyl ether
PCE	Perchloroethene
TCE	Trichloroethene
TOC	Top of casing
URL	Uniform Resource Locator
WL	Wilke and Lee Method for Air Diffusion

Appendix 3 Plume Diving Calculator Equations

Phreatic Surface

The first solution is used to determine the location of the phreatic surface Bear (1972, page 379) and is given by

$$h^2 = -\frac{N}{K} + Cx + B \tag{19}$$

where h is the elevation of the phreatic surface above the datum (bottom of the aquifer) [L], N is the recharge rate [$L^3/L^2/T$], K is the hydraulic conductivity of the aquifer [L/T], x is the distance [L]. The constants C and B in equation 19 are determined from

$$C = \frac{h_1^2 - h_2^2 - \frac{N}{K}(x_2^2 - x_1^2)}{x_1 - x_2} \tag{20}$$

and

$$B = h_2^2 + \frac{N}{K}x_2^2 - Cx_2 \tag{21}$$

where x_1 and x_2 [L] are up and down gradient locations in the aquifer, and h_1 and h_2 [L] are the corresponding phreatic surface elevations or heads. Bear's solution does not require that the water table elevation decrease monotonically down gradient. Depending on the values input for recharge, hydraulic conductivity and heads, there could be a ground water divide between the two specified end points.

Aquifers Composed of Multiple Segments

If an aquifer can be conceptualized as being composed of a set of segments, then different properties can be applied to each while still using the analytic solution given for the water table Bear (1972). In concept, this is the same idea that underlies the analytic element method Haitjema (1995). Of particular interest are situations where the recharge varies over the site. By supplying differing recharge rates to segments of the model, the effects of localized recharge variation can be incorporated intoan analytic solution. The coefficients, C and B, which are determined for each segment, are chosen to satisfy continuity of head and flux as the segment boundaries are crossed. Since there can be no jump in head across segment boundaries,

$$h_{sb} \quad = \quad - \frac{N_i}{K_i} x_{sb}^2 \ + \ C_i x_{sb} \ + \ B_i$$

$$= \quad - \frac{N_{i+1}}{K_{i+1}} x_{sb}^2 \ + \ C_{i+1} x_{sb} \ + \ B_{i+1} \qquad\qquad (22)$$

where x_{sb} and h_{sb} are the position and the head of the segment boundary, respectively. The flux condition is given by

$$q_{sb} \quad = \quad - (K_i \frac{dh}{dx})_i \quad = \quad - (K_{i+1} \frac{dh}{dx})_{i+1} \qquad\qquad (23)$$

where q_{sb} is the flux across the segment boundary. A consequence of this formulation is that there is a jump in gradient across the segment boundaries if the hydraulic conductivities differ. For each pair of segments there are two conditions that are applied where the segments join, and two conditions applied at exterior edges. Since the equations are linear, they can be solved using gaussian elimination.

The recharge model is based on the assumption that the aquifer can be conceptualized as a one-dimensional flow system. It is easy to generate parameter sets that result in mounding in the middle of the domain--*reducing* the hydraulic conductivity and *increasing* the recharge rate for the center section. The result is that there is flow toward *both* ends of the domain. This occurs even though one head is higher than the other. It is the volume of water entering the aquifer from all sources that determines the shape of the water table. In this case there can be enough water entering through recharge swamp out the gradient that would be established by the constant head boundaries.

By changing the hydraulic conductivity to 0.1 ft/d and increasing the recharge rate to 20 in/yr, a mound is generated in the example problem solution. Flow is toward the left hand boundary (50 ft head) when the source location is chosen to be 275 ft (Figure 36).
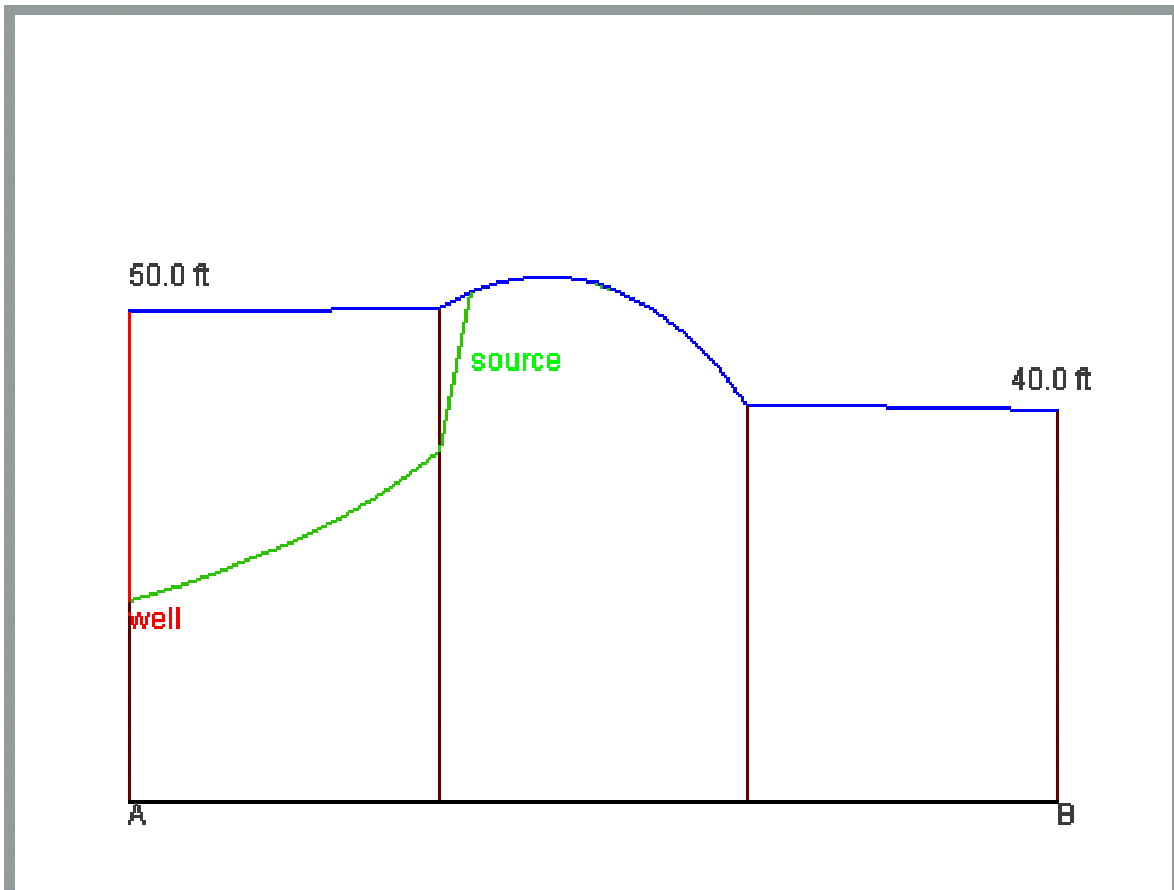
Figure 36 Water table mounding due to unequal recharge and hydraulic conductivity.

If the mounding is caused by a localized source, for example, a gravel pit, then the flow system might really be two- or three-dimensional. In this case flow might go around the mound. The one-dimensional mounding case is more realistic for large scale recharge zones as would occur because of topography.

Appendix 4 One-Dimensional Transport in a Homogeneous Aquifer

The first arrival time, maximum concentration and durations are calculated from the transport equation. Transport in a one-dimensional homogeneous aquifer is governed by

$$R \frac{\partial c}{\partial t} = -v_x \frac{\partial c}{\partial x} + D_x \frac{\partial^2 c}{\partial x^2} + D_y \frac{\partial^2 c}{\partial y^2} + D_z \frac{\partial^2 c}{\partial z^2} - \lambda c \qquad (24)$$

where R is the retardation factor [dimensionless], c is the concentration [M/L^3]; t represents time [T]; x, y, and z are the three cartesian coordinate directions [L]; v_x, is the x-direction seepage velocity [L/T], D_x, D_y and D_x are the three components of dispersion [L^2/T], and λ is a first order loss coefficient [T^{-1}]. This form of the transport equation is based on the assumption that the dispersion constants are independent of time and space that ground water flow is one-dimensional, steady and uniform, that biodegradation is adequately represented by a first order process.   With boundary conditions specified as

$$c(0) = \begin{array}{l} c_o \; ; \; t < t_p \\ 0 \; ; \; t > t_p \end{array}$$

$$\frac{dc}{dx}(\infty) = 0 \qquad (25)$$

a solution can be obtained for a one-dimensional case where the transverse and vertical components of dispersion are assumed negligible (van Genuchten and Alves, 1982) or a similar three dimensional case (Leij and Bradford, 1994).   The one-dimensional case is useful because of rapid computation of its results and is used in the following.

The solution for the one-dimensional case is

$$c(x,t) = c_o(B(x,t) - B(x,t - t_o)) \qquad (26)$$

where B(x,t) is defined by

$$B(x,t) = \frac{1}{2} \exp\left(\frac{v - u}{2D}\right) \mathrm{erfc} \frac{Rx - ut}{2\sqrt{DRt}}$$

$$+ \frac{1}{2} \exp\left(\frac{v + u}{2D}\right) \mathrm{erfc} \frac{Rx + ut}{2\sqrt{DRt}} \qquad (27)$$

and u is defined as

$$u = v\sqrt{1 + \frac{4\lambda D}{v^2}} \qquad\qquad (28)$$

Appendix 5 Estimation of Temperature-Dependent Henry's Law Coefficients

Two methods are used to calculate the temperature-dependence of Henry's law coefficients. First is a method used to adjust the values using the Clausius-Clapeyron relationship:

$$H_{TS} = H_R \exp\left[\frac{-\Delta H_{v,TS}}{R_C}\left(\frac{1}{T_S} - \frac{1}{T_R}\right)\right] \tag{29}$$

where H_{TS} is the dimensional (atm-m^3/mol) Henry's Law coefficient at the Kelvin temperature, T_S, $\Delta H_{v,TS}$ is the enthalpy of vaporization at T_S in units of cal/mol, T_R is the reference temperature for Henry's Law (H_R) in K, and R_C is the gas constant and is equal to 1.9872 cal/mol-K. The enthalpy of vaporization, $\Delta H_{v,TS}$ is estimated from

$$\Delta H_{v,TS} = \Delta H_{v,b}\left[\frac{1 - T_S/T_C}{1 - T_B/T_C}\right]^n \tag{30}$$

where $\Delta H_{v,b}$ is the enthalpy of vaporization at the normal boiling point (cal/mol), T_B is the normal boiling point in K, and T_C is the critical temperature in K. The exponent n is selected from Table 24

Ratio T_B/T_C	Exponent n
< 0.57	0.30
0.57 to 0.71	0.74 (T_B/T_C) - 0.116
> 0.71	0.41

Table 24 Exponent "n" used in calculation of enthalpy of vaporization.

All of the input values required for these equations were generated by the US EPA Office of Solid Waste and Emergency Response (OSWER) and are available in a fact sheet (US EPA, 2001). The fact sheet contains more information on these methods. Notably the normal boiling point enthalpies of vaporization ($\Delta H_{v,b}$) were estimated from the Antoine equation for vapor pressure. The coefficients of the Antoine equation were themselves estimated from methods given in the factsheet. These quantities are not recalculated in the Henry's law calculator because they were tabulated in the attachment to the OSWER factsheet.

The second method was developed by Washington (1996). For many compounds included in this calculator, variation of Henry's Law Constant with temperature is quantified by the van't Hoff Equation:

$$\ln K_h \quad = \quad \frac{-\,\Delta H_r^{\ominus}}{R\,T} \;+\; \frac{\Delta S_r^{\ominus}}{R} \tag{31}$$

where $\ln K_h$ is the natural logarithm of the Henry's constant, ΔH_r^{θ} is the standard state enthalpy, R is the universal gas constant, T is the temperature in Kelvin, and ΔS_r^{θ} standard state entropy. This method is based upon the assumption that the head capacity is the same for the reactants and products. Therefore the temperature range is not extrapolated beyond values used in generating the coefficients used in making the estimates.

Appendix 6 Diffusion Coefficients

The Fuller, Schettler and Giddings (FSG) method is based on the regression formula:

$$D_{BA} \ = \ \frac{0.001 \, T^{1.75} \, \sqrt{M_r}}{P \, (V_A \, + \, V_B)^2} \tag{32}$$

where D_{BA} is the diffusion coefficient of compound B in compound A in cm^2/s, T is the temperature in K, P is the pressure in atm, M_r a function of the molecular weights M_A and M_B of compounds A and B, V_A and V_B are the molar volumes of air (A) and the gas (B) in question. M_r is equal to $(M_A + M_B)/M_A M_B$. V_B can be estimated from volume increments associated with each element in the compound. These increments give the volume (cm^3) per mole of atom present. The values are given in the reference and have been programmed into the calculator.

The FSG-LaBas method uses the same formula as the FSG method but substitutes the LaBas volume estimates for molar volume. The FSG-LaBas method allows for estimating the diffusivities of more compounds of interest.

The Wilke and Lee (WL) method uses LaBas molar volumes and is based upon a series of calculations of a "collision integral", Ω, that represents collision between atoms. The estimate of D_{BA} is given by

$$D_{BA} \ = \ \frac{B' \, T^{3/2} \, \sqrt{M_r}}{P \, s^2_{AB} \, \Omega} \tag{33}$$

where B' is a function of the molecular weights of A, s^2_{BA} is the average molal volume at the boiling point of A and B, and Ω is called the collision integral. The details of calculation of these quantities are given (Tucker and Nelken, 1990).

Diffusion Coefficients in Water

The Hayduk and Laudie (HL) method for estimating the diffusivity of an organic compound in water in cm^2/s is given by

$$D_{BW} \ = \ \frac{13.26 \, x \, 10^{-5}}{n_w^{1.14} \, V_B^{0.589}} \tag{34}$$

where D_{BW} is the diffusion coefficient of compound B in compound A (water) in cm^2/s, n_w is the viscosity of water in cp (corrected for temperature) and V_B are the LaBas molar volume increments.